NASA
Contractor Report 4704

Army Research Laboratory
Contractor Report ARL-CR-287

Computerized Design and Analysis of Face-Milled, Uniform Tooth Height, Low-Noise Spiral Bevel Gear Drives

F.L. Litvin and X. Zhao

GRANT NAG3-1607
JANUARY 1996

National Aeronautics and Space Administration

U.S. ARMY RESEARCH LABORATORY

NASA
Contractor Report 4704

Army Research Laboratory
Contractor Report ARL-CR-287

Computerized Design and Analysis of Face-Milled, Uniform Tooth Height, Low-Noise Spiral Bevel Gear Drives

F.L. Litvin and X. Zhao
University of Illinois at Chicago
Chicago, Illinois

Prepared for
Propulsion Directorate
U.S. Army Aviation Systems Command
and
Lewis Research Center
under Grant NAG3-1607

National Aeronautics and
Space Administration
Office of Management
Scientific and Technical
Information Program
1996

Abstract

A new method for design and generation of spiral bevel gears of uniform tooth depth with localized bearing contact and low level of transmission errors is considered.

The main features of the proposed approach are as follows:

(1) The localization of the bearing contact is achieved by the mismatch of the generating surfaces. The bearing contact may be provided in the longitudinal direction, or in the direction across the surface.

(2) The low level of transmission errors is achieved due to application of nonlinear relations between the motions of the gear and the gear head-cutter. Such relations may be provided by application of a CNC machine. The generation of the pinion is based on application of linear relations between the motions of the tool and the pinion being generated. The relations described above permit a parabolic function of transmission errors to be obtained that is able to absorb almost linear functions caused by errors of gear alignment.

A computer code has been written for the meshing and contact of the spiral bevel gears with the proposed geometry. The effect of misalignment on the proposed geometry has also been determined. Numerical examples for illustration of the proposed theory have been provided.

TABLE OF CONTENTS

1 Introduction

The research project is directed at the design and generation of face-milled spiral bevel gears with the following features:

(1) The depth of the teeth is uniform which means that the height of the teeth is constant.

(2) The gear tooth surfaces contact each other at every instant at a point. Thus, the bearing contact is localized and therefore the sensitivity of the gears to misalignment is reduced.

(3) The surface contact under the load is spread over an elliptical area, whose center is the theoretical contact point. The set of instantaneous contact ellipses form the bearing contact. The developed methods of synthesis provide two types of bearing contact that may be directed: (i) in the longitudinal direction, or (ii) across the tooth surface.

(4) Two generating surfaces, Σ_c and Σ_c, are used for the generation of the pinion and the gear tooth surfaces Σ_1 and Σ_2, respectively. The dimensions of the instantaneous contact ellipse depend on the load applied to the gear drive, and on the chosen relation between the curvatures of the generating surfaces.

(5) Gear misalignment may cause transmission errors of a high level and of such a s[illegible] that a high level of vibration will be resulted. The developed approach provides at each cycle of meshing a predesigned parabolic function that will absorb the transmission errors caused by misalignment. The cycle of meshing is determined as

$$\phi_1 = \frac{2\pi}{N_1} \tag{1}$$

where ϕ_1 and N_1 are the angle of pinion rotation and the pinion tooth number.

2 Method for Generation of Conjugated Pinion-Gear Tooth Surfaces

Kinematic Relations

We will consider initially an imaginary process for generation when the pinion and gear tooth surfaces will be generated simultaneously. Such an approach will permit one to obtain: (i) important kinematic relations to be executed on the CNC machine, and (ii) to visualize the possibility to obtain two kinds of the localized bearing contact. In reality, the pinion and gear tooth surfaces are generated separately as it is discussed in the following sections.

We start with the case when the axes of the pinion and the gear form an angle of 90° (fig. 1). However, the developed approach is applicable for gear drives whose shaft angle differs of 90°. The pinion and the gear during the process for generation perform rotation about axes X_{d_1} and X_{d_2}, respectively. Two rigidly connected generating surfaces, Σ_t and Σ_c, perform rotation about the Z_m axis. Surfaces Σ_t and Σ_c generate the pinion and gear tooth surfaces Σ_1 and Σ_2, respectively. The relation between the angular velocities $\omega^{(1)}$ and $\omega^{(c)}$ is represented by the equation

$$\frac{\omega^{(c)}}{\omega^{(1)}} = \sin\gamma_1 \tag{2}$$

where γ_1 is the pitch angle of the pinion. The transmission function of the gear drive must be obtained for each cycle of meshing as the sum of the theoretical linear function and the predesigned parabolic function as shown in fig. 2. We may represent the transmission function at the first cycle of meshing by the equation

$$\phi_2 = \frac{N_1}{N_2}\phi_1 - a\phi_1^2 \quad (-\frac{\pi}{N_1} \leq \phi_1 \leq \frac{\pi}{N_1}) \tag{3}$$

Differentiating equation (3), we obtain that

$$\omega^{(2)} = (\frac{N_1}{N_2} - 2a\phi_1)\omega_1 \tag{4}$$

Taking into account (see equation (2)) that

$$\phi_1 = \frac{\phi_c}{\sin\gamma_1} \tag{5}$$

we obtain that

$$\phi_2 = \frac{N_1}{N_2 \sin\gamma_1}\phi_c - a(\frac{\phi_c}{\sin\gamma_1})^2 \tag{6}$$

$$\omega^{(2)} = (\frac{N_1}{N_2} - \frac{2a\phi_c}{\sin\gamma_1})(\frac{\omega^{(c)}}{\sin\gamma_1}) \tag{7}$$

Considering ϕ_c and ω_c as the input parameters, we may obtain $\omega^{(1)}$, ϕ_1, ϕ_2, and $\omega^{(2)}$ using equations (2), (5), (6), and (7), respectively. Since $\phi_2(\phi_c)$ is a nonlinear function, the generation of the gear requires application of a CNC machine for the execution of the nonlinear function $\phi_2(\phi_c)$.

Note: The ratio of $\omega^{(1)}$ and $\omega^{(t)}$ ($\omega^{(t)} = \omega^{(c)}$) is constant during the process of pinion generation, the instantaneous axis of rotation is directed along the X_m axis, and the pinion axode (in the process of meshing of the pinion tooth surface Σ_1 with the generating surface Σ_t) is a circular cone with the pitch angle

$$\tan\gamma_1 = \frac{N_1}{N_2} \tag{8}$$

The axode of the generating surface is the plane $Z_m = 0$ that is tangent to the pinion axode.

The ratio of angular velocities $\frac{\omega^{(2)}}{\omega^{(t)}}$, and $\frac{\omega^{(2)}}{\omega^{(c)}}$ is not constant. Therefore, the axode of gear 2 being in meshing with the pinion and the generating surface Σ_c is not a circular cone.

Generating Surfaces

It was mentioned above that two rigidly connected generating surfaces Σ_t and Σ_c are applied for the generation of the pinion and gear, respectively. Two pairs of surfaces Σ_t and Σ_c are applied to provide two types of bearing contact for the generated pinion and gear tooth surfaces Σ_1 and Σ_2.

Case 1:

The two generating surfaces are a cone Σ_t and a surface of revolution Σ_c. The surfaces are in tangency along a circle and are rigidly connected each to other in the process for generation (fig. 3). Surfaces Σ_c and Σ_2 are in line tangency along lines L_{c_2} while being in mesh in the process for generation. Similarly, Σ_t and Σ_1 are in line contact along lines L_{t1} (not shown in fig. 3). However, instantaneous contact lines L_{c_2} and L_{t1} do not coincide each with other but are in tangency at a point that belongs to the circle L_{ct}. This means that surfaces Σ_1 and Σ_2 are in point contact at every instant that moves along the circular arc L_{ct} in the process of meshing. The path of contact L_{ct} (and the bearing contact) has a longitudinal direction.

Case 2:

The generating surfaces Σ_c and Σ_t are rigidly connected cones that are in tangency along their common generatrix L_{ct} (fig. 4). Only contact lines L_{c_2} between surfaces Σ_c and Σ_2 are shown in the figure. Each contact line L_{c_2} and the respective line L_{t1} are in tangency at the respective point of the generatrix L_{ct}. This point is the current point of tangency of gear

tooth surfaces Σ_1 and Σ_2.

The generating surfaces Σ_t and Σ_c are the surfaces of two head-cutters that are applied for the generation of the pinion and the gear, respectively. In reality, the head-cutters are provided with straight line blades or with circular arc edge blades but not with surfaces. Such blades are rotated about the head- cutter axes to form the generating surfaces. The angular velocity of rotation of blades must provide the required velocity of cutting or grinding, but is not related with the process for generation of the pinion or gear tooth surfaces.

The head-cutter is installed on the cradle of the cutting machine and then performs with the cradle the rotation about the Z_m axis with the angular velocity $\omega^{(c)} = \omega^{(t)}$. Details of the settings of the head-cutter on the cradle are discussed in sections 3 and 4.

3 Generation of Gear Tooth Surfaces

Applied Coordinate Systems and Machine-Tool Settings

We have considered in Section 2 an imaginary process of generation of conjugate pinion-gear tooth surfaces based on the assumption that the surfaces will be generated simultaneously. In reality, the pinion-gear tooth surfaces are generated separately, as it was mentioned above.

This section deals with gear generation and the applied machine-tool settings. The gear tooth surfaces are generated by a head-cutter that is provided with straight-line blades (fig. 5). Both sides of the gear tooth are generated simultaneously. The blades are rotated about the head-cutter axis. The edges of rotated blades form two circular cones as the generating surfaces used for the manufacturing of the gear.

Henceforth, we will apply the movable coordinate systems S_{c_2} and S_2 that are rigidly

connected to the cradle and the gear, respectively (fig. 6). The fixed coordinate system S_m is rigidly connected to the cutting machine. Coordinate system S_{d_2} is an additional fixed one and is rigidly connected to the coordinate system S_m. The orientation of S_{d_2} with respect to S_m is determined by angle $\gamma_2 = \gamma - \gamma_1$, where γ_1 is the pitch angle of the pinion pitch cone. During the process for generation, the cradle and the gear perform related rotations about the X_m-axis and the X_{d_2}-axis, respectively. The current angles of rotation of the cradle and the gear are designated by ϕ_{c_2} and ϕ_2, that are related by equation (6) in which we change the designation of ϕ_c for ϕ_{c_2}. This relation provides the predesigned parabolic function designated for the absorption of transmission errors caused by misalignment.

The installment of the head-cutter is shown in fig. 7(a). Figure 7(a) shows the position of the cradle when $\phi_{c_2} = 0$, and the coordinate system S_{c_2} coincides with S_m. Coordinate system S_{p_2} is an additional coordinate system that is rigidly connected to S_{c_2}, and performs rotation with S_{c_2} as shown in fig. 7(b). Coordinate axes of S_{p_2} and S_{c_2} have the same orientation. Axis Z_{p_2} is the axis of the head-cutter (see below). The installment of the head-cutter in S_{c_2} may be determined by the parameters of the triangle with the apexes O_{c_2}, O_{p_2}, and M, where M is the mean point of the cone distance of gear 2 (fig. 8). The installment of the head- cutter in coordinate system S_{c_2} may be determined as well by H_G and V_G (fig. 8), where

$$H_G = A_m - R_{u2} \sin \beta_2 \tag{9}$$

$$V_G = R_{u2} \cos \beta_2 \tag{10}$$

Here, $R_{u2} = |\overline{O_{p_2} M}|$ is the nominal radius of the head-cutter (fig. 8), $A_m = |\overline{O_{c_2} M}|$, and β_2 is the spiral angle of the gear. Alternative coupled parameters of installment, $S_{r2} = |\overline{O_{c_2} O_{p_2}}|$ and q_2, H_G and V_G, are related by the equations

$$S_{r2} = (H_G^2 + V_G^2)^{0.5} \tag{11}$$

$$q_2 = \tan^{-1}(\frac{V_G}{H_G}) \tag{12}$$

Equations of Gear Generating Surfaces

We have mentioned before that two cones as generating surfaces are used for cutting of the space of the gear (fig. 5). Fig. 9(b) shows the cutting blade, and fig. 9(a) shows one of the generating cones. The generating cone is formed by rotation of the blade edge about the Z_{p_2} axis. The equations of the cone are represented in S_{p_2} as

$$\mathbf{r}_{p_2}(S_G, \theta_G) = \begin{bmatrix} (r_c - S_G \sin\alpha_G)\cos\theta_G \\ (r_c - S_G \sin\alpha_G)\sin\theta_G \\ -S_G \cos\alpha_G \end{bmatrix} \tag{13}$$

where θ_G and S_G (fig. 9(a)) are the surface coordinates (the Gausian coordinates); α_G is the blade angle; r_c is the radius of the head-cutter that is measured at the tip of the blade. Parameters r_c and R_{u2} are related as follows

$$r_c = R_{u2} \pm \frac{PW}{2} \tag{14}$$

The upper and lower signs in (14) correspond to the gear concave and convex sides. Equations (13) may represent both generating cones, if we will use the rule of signs in equation (14), and consider that $\alpha_G > 0$ and $\alpha_G < 0$ correspond to the gear concave and convex sides, respectively.

The unit normal to the gear generating surface is represented by the equations

$$\mathbf{n}_{p_2} = \frac{\mathbf{N}_{p_2}}{|\mathbf{N}_{p_2}|}, \quad \mathbf{N}_{p_2} = \frac{\partial \mathbf{r}_{p_2}}{\partial \theta_G} \times \frac{\partial \mathbf{r}_{p_2}}{\partial S_G} \tag{15}$$

Equations (14) and (15) yield

$$\mathbf{n}_{p_2}(\theta_G) = \begin{bmatrix} -\cos\alpha_G \cos\theta_G \\ -\cos\alpha_G \sin\theta_G \\ \sin\alpha_G \end{bmatrix} \tag{16}$$

Algorithm for Derivation of Gear Tooth Surfaces

The derivation of gear tooth surface Σ_2 is based on the following procedure:

Step 1:

Initially we derive the family of generating surfaces in S_2 using the matrix equation

$$\begin{aligned} \mathbf{r}_2(S_G, \theta_G, \phi_{c_2}) &= \mathbf{M}_{2p_2}\mathbf{r}_{p_2}(S_G, \theta_G) \\ &= \mathbf{M}_{2d_2}(\phi_2)\mathbf{M}_{d_2m}\mathbf{M}_{mc_2}(\phi_{c_2})\mathbf{M}_{c_2p_2}\mathbf{r}_{p_2}(S_G, \theta_G) \end{aligned} \tag{17}$$

where ϕ_2 and ϕ_{c_2} are related by equation (6).

Step 2:

Then, we derive the equation of meshing between the gear and the generating surface that we represent in the form

$$\mathbf{n}_m^{(p_2)} \cdot \mathbf{v}_m^{(p_2 2)} = f(S_G, \theta_G, \phi_{c_2}) = 0 \tag{18}$$

where $\mathbf{n}_m^{(p_2)}$ is the unit normal to the generating surface Σ_{p_2}, and $\mathbf{v}^{(p_2 2)}$ is the relative (sliding) velocity. The scaler product $(\mathbf{n}^{(p_2)} \cdot \mathbf{v}^{(p_2 2)})$ may be represented in any coordinate system. In our derivations, the scaler product is represented in S_m.

Note: we may represent as well the equation of meshing in the form

$$\mathbf{N}_m^{(p_2)} \cdot \mathbf{v}_m^{(p_2 2)} = 0 \tag{19}$$

where $\mathbf{N}^{(p_2)}$ is the normal but not the unit normal to the generating surface.

Equations (17) and (18), considered simultaneously, represent the gear tooth surface as the envelope to the family (17) of generating surfaces.

Derivation of Family of Surfaces (17)

Vector function $\mathbf{r}_{p_2}(S_G, \theta_G)$ has been already represented by (13). Matrices in equation (17) are represented as follows (see figs. 6,7, and 8)

$$\mathbf{M}_{2d_2} = \begin{bmatrix} 1 & 0 & 0 & 0 \\ 0 & \cos\phi_2 & \sin\phi_2 & 0 \\ 0 & -\sin\phi_2 & \cos\phi_2 & 0 \\ 0 & 0 & 0 & 1 \end{bmatrix} \tag{20}$$

$$\mathbf{M}_{d_2 m} = \begin{bmatrix} \cos\gamma_2 & 0 & \sin\gamma_2 & 0 \\ 0 & 1 & 0 & 0 \\ -\sin\gamma_2 & 0 & \cos\gamma_2 & 0 \\ 0 & 0 & 0 & 1 \end{bmatrix} \tag{21}$$

$$\mathbf{M}_{mc_2} = \begin{bmatrix} \cos\phi_{c_2} & -\sin\phi_{c_2} & 0 & 0 \\ \sin\phi_{c_2} & \cos\phi_{c_2} & 0 & 0 \\ 0 & 0 & 1 & 0 \\ 0 & 0 & 0 & 1 \end{bmatrix} \tag{22}$$

Equations (17) and (20)–(22) represent the family of generating surfaces in form of three parameters. The relation between these parameters is represented by the equation of meshing (18).

Derivation of Equation of Meshing

We represent in coordinate system S_m the unit normal $\mathbf{n}_m^{(p_2)}$ to the generating surface using the following matrix equation

$$\mathbf{n}_m^{(p_2)}(\theta_G, \phi_2) = \mathbf{L}_{mc_2}\mathbf{L}_{c_2 p_2}\mathbf{n}_{p_2}(\theta_G) \tag{23}$$

Here:

Vector function $\mathbf{n}_{p_2}(\theta_G)$ is represented by equation (16). Matrix L is the 3×3 submatrix of the 4×4 matrix M. After derivations, we obtain

$$\mathbf{n}_m(\theta_G, \phi_{c_2}) = \begin{bmatrix} -\cos\alpha_G \cos(\theta_G + \phi_{c_2}) \\ -\cos\alpha_G \sin(\theta_G + \phi_{c_2}) \\ \sin\alpha_G \end{bmatrix} \tag{24}$$

As a reminder, the variables ϕ_2 and ϕ_{c_2} are related by equation (6).

The derivation of the relative velocity $\mathbf{v}^{(p_2 2)}$ is based on the following considerations

Step 1:

We represent vector $\mathbf{v}_m^{(p_2 2)}$ as follows

$$\mathbf{v}_m^{(p_2 2)} = (\omega_m^{(p_2)} - \omega_m^{(2)}) \times \mathbf{r}_m^{(c_2)} \tag{25}$$

where

$$\omega_m^{(p_2)} = [0 \;\; 0 \;\; \omega^{(c_2)}]^T \tag{26}$$

$$\omega_m^{(2)} = \mathbf{L}_{m2}\omega^{(2)} = \mathbf{L}_{md_2}\mathbf{L}_{d_2 2}\omega^{(2)} = [\omega^{(2)}\cos\gamma_2 \;\; 0 \;\; \omega^{(2)}\sin\gamma_2]^T \tag{27}$$

The relation between $\omega^{(p_2)}$ and $\omega^{(2)}$ may be obtained by differentiating equation (6) that yields

$$\omega^{(2)} = \frac{N_1}{N_2 \sin\gamma_1}\omega^{(c_2)} - 2a\left(\frac{\phi_{c_2}}{\sin\gamma_1}\right)\frac{\omega^{(c_2)}}{\sin\gamma_1} \tag{28}$$

4 Machine-Tool Settings for Pinion Generation

Introduction

Henceforth, we will consider methods for the pinion generation that provide two types of the path of contact : across the surface and along the surface. The developed machine-tool settings will be determined: (i) for the imaginary process for generation based on application of two rigidly connected generating surfaces (see figs. 3 and 4), and (ii) machine-tool settings represented in terms of the Gleason Works terminology.

Coordinate Systems Applied for Pinion Generation

Movable coordinate systems S_{c_1} and S_1 are rigidly connected to the cradle of the cutting machine and the pinion, respectively (fig. 10). An auxiliary coordinate system S_{p_1} is rigidly connected to the head-cutter and the cradle. Axes of coordinate systems S_{c_1} and S_{p_1} have the same orientation. Fixed coordinate systems S_m

and S_{d_1} are rigidly connected to the cutting machine. The pinion and the cradle perform rotation about axes x_{d_1} and z_m, respectively. During the generation, the cradle and the pinion are rotated uniformly, and the angles of rotation are related as follows :

$$\phi_{c_1} = \phi_1 \sin\gamma_1 \tag{29}$$

where γ_1 is the pinion pitch angle.

Pinion Machine-Tool Settings

The pinion machine-tool settings for the imaginary process of generation are determined by the following set of parameters (fig. 10): γ_1, S_{r1} and q_1. The machine-tool settings for the real process of generation may be determined by turning of systems S_1, S_{d_1}, S_{p_1} and S_{c_1} at 180° about the x_m-axis. Fig. 11 shows the installment of the pinion on the cutting machine and its rotation during the process for generation. Fig. 12(a) shows the initial installment of the head-cutter and cradle and fig. 12(b) shows the rotation of the cradle during the process for generation (fig. 12(b)).

5 Equations of Pinion Tooth Surfaces

Orientation of Bearing Contact Across Surface

The mentioned type of bearing contact is provided by application of two rigidly connected circular cones that generate the gear and pinion tooth surface, respectively (fig. 4). Fig. 13 shows the cross sections of the surfaces of the pinion and gear head-cutters in plane $z_m = 0$ when the cradle is at the initial position that is determined with $\phi_{c_1} = 0$, and the coordinate systems S_{c_1} and S_m coincide each with other (fig. 10(b)).

Fig. 14 shows the profiles of the cutter blades used for the generation of the pinion concave side and convex side surfaces, respectively. Fig. 15 shows the generating surface (cone) in system S_{p_1}. The derivation of the generated pinion tooth surface is based on the following procedure.

Step 1:

The head-cutter generating surface is represented in S_{p_1} as

$$\mathbf{r}_{p_1} = \begin{bmatrix} (r_{cp} - S_p \sin\alpha_p)\cos\theta_p \\ (r_{cp} - S_p \sin\alpha_p)\sin\theta_p \\ -S_p \cos\alpha_p \\ 1 \end{bmatrix} \tag{30}$$

Here, r_{cp} is the point radius (fig. 14), α_p is the blade angle. The sign of α_p should be considered as positive and negative when the pinion convex and concave tooth surfaces are generated, respectively. Parameters θ_p and S_p are the head-cutter surface parameters.

The unit normal of the head-cutter generating surface is represented in S_{p_1} as

$$\mathbf{n}_{p_1} = \frac{\mathbf{N}_{p_1}}{|\mathbf{N}_{p_1}|} \; ; \quad \mathbf{N}_{p_1} = \frac{\partial \mathbf{r}_{p_1}}{\partial \theta_p} \times \frac{\partial \mathbf{r}_{p_1}}{\partial s_p} \tag{31}$$

Equations (30) and (31) yield

$$\mathbf{n}_{p_1} = \begin{bmatrix} -cos\alpha_p \cos\theta_p \\ -cos\alpha_p \sin\theta_p \\ \sin\alpha_p \end{bmatrix} \tag{32}$$

Step 2:

The family of head-cutter generating surfaces is represented in S_1 by the matrix equation

$$\mathbf{r}_1(S_p, \theta_p, \phi_{c_1}) = \mathbf{M}_{1d_1}\mathbf{M}_{d_1m}\mathbf{M}_{mc_1}\mathbf{M}_{c_1p_1}\mathbf{r}_{p_1}(S_p, \theta_p) \tag{33}$$

Here,

$$\mathbf{M}_{1d_1} = \begin{bmatrix} 1 & 0 & 0 & 0 \\ 0 & \cos\phi_1 & \sin\phi_1 & 0 \\ 0 & -\sin\phi_1 & \cos\phi_1 & 0 \\ 0 & 0 & 0 & 1 \end{bmatrix} \tag{34}$$

$$\mathbf{M}_{d_1m} = \begin{bmatrix} \cos\gamma_1 & 0 & \sin\gamma_1 & 0 \\ 0 & 1 & 0 & 0 \\ -\sin\gamma_1 & 0 & \cos\gamma_1 & 0 \\ 0 & 0 & 0 & 1 \end{bmatrix} \tag{35}$$

$$\mathbf{M}_{mc_1} = \begin{bmatrix} \cos\phi_{c_1} & -\sin\phi_{c_1} & 0 & 0 \\ \sin\phi_{c_1} & \cos\phi_{c_1} & 0 & 0 \\ 0 & 0 & 1 & 0 \\ 0 & 0 & 0 & 1 \end{bmatrix} \tag{36}$$

$$\mathbf{M}_{c_1p_1} = \begin{bmatrix} 1 & 0 & 0 & S_{r1}\cos q_1 \\ 0 & 1 & 0 & S_{r1}\sin q_1 \\ 0 & 0 & 1 & 0 \\ 0 & 0 & 0 & 1 \end{bmatrix} \tag{37}$$

Step 3:

The equation of meshing is represented in system S_m as

$$\mathbf{n}_m \cdot \mathbf{v}_m^{(c_1 1)} = 0 \tag{38}$$

Here,

$$\mathbf{n}_m(\theta_p, \phi_{c_1}) = \begin{bmatrix} n_{xm} \\ n_{ym} \\ n_{xm} \end{bmatrix} = \mathbf{L}_{mc_1}\mathbf{L}_{c_1p_1}\mathbf{n}_{c_1}(\theta_p) \tag{39}$$

$$\mathbf{v}_m^{(c_1 1)} = \boldsymbol{\omega}_m^{(c_1 1)} \times \mathbf{r}_m \tag{40}$$

where

$$\begin{aligned} \mathbf{r}_m &= \mathbf{M}_{mc_1}\mathbf{M}_{c_1p_1}\mathbf{r}_{p_1} \\ &= \begin{bmatrix} -S_p \sin\alpha_p \cos(\theta_p + \phi_{c_1}) + r_{cp}\cos(\theta_p + \phi_{c_1}) + S_{r1}\cos(\phi_{c_1} + q_1) \\ -S_p \sin\alpha_p \sin(\theta_p + \phi_{c_1}) + r_{cp}\sin(\theta_p + \phi_{c_1}) + S_{r1}\sin(\phi_{c_1} + q_1) \\ -S_p \cos\alpha_p \end{bmatrix} \end{aligned} \tag{41}$$

Using the designations

$$\left.\begin{aligned} B_1 &= r_{cp}\cos(\theta_p + \phi_{c_1}) + S_{r1}\cos(\phi_{c_1} + q_1) \\ B_2 &= r_{cp}\sin(\theta_p + \phi_{c_1}) + S_{r1}\sin(\phi_{c_1} + q_1) \end{aligned}\right\} \tag{42}$$

we obtain

$$\mathbf{r}_m = \begin{bmatrix} -S_p \sin\alpha_p \cos(\theta_p + \phi_{c_1}) + B_1 \\ -S_p \sin\alpha_p \sin(\theta_p + \phi_{c_1}) + B_2 \\ -S_p \cos\alpha_p \end{bmatrix} \tag{43}$$

$$\omega_m^{(c_1 1)} = \omega_m^{(c_1)} - \omega_m^{(1)} = \begin{bmatrix} 0 \\ 0 \\ \omega_{c_1} \end{bmatrix} - \begin{bmatrix} \omega_1 \cos\gamma_1 \\ 0 \\ \omega_1 \sin\gamma_1 \end{bmatrix} = \begin{bmatrix} \omega_1 \cos\gamma_1 \\ 0 \\ 0 \end{bmatrix} \tag{44}$$

Then, we obtain that (since $\omega_{c_1} = \omega_1 \sin\gamma_1$)

$$\mathbf{v}_m^{(c_1 1)} = \omega_m^{(c_1 1)} \times \mathbf{r}_m = \begin{bmatrix} 0 \\ S_p \cos\alpha_p \cos\gamma_1 \\ -S_p \sin\alpha_p \sin(\theta_p + \phi_{c_1})\cos\gamma_1 + B_2 \cos\gamma_1 \end{bmatrix} \tag{45}$$

We have assumed not loosing the generality of the approach that $|\omega_1| = 1$.

The equation of meshing yields

$$n_{ym} S_p \cos\alpha_p \cos\gamma_1 - n_{zm} S_p \sin\alpha_p \sin(\theta_p + \phi_{c_1})\cos\gamma_1 + n_{zm} B_2 \cos\gamma_1 = 0 \tag{46}$$

or

$$S_p(\theta_p, \phi_{c_1}) = \frac{-n_{zm} B_2}{n_{ym}\cos\alpha_p - n_{zm}\sin\alpha_p \sin(\theta_p + \phi_{c_1})} \tag{47}$$

Step 4:

The envelope to the family of generating surfaces may be represented in two parameter form if we eliminate in equation (33) parameter S_p using equation (47).

Orientation of Bearing Contact in Longitudinal Direction

The mentioned orientation of the bearing contact can be achieved by application of generating surfaces shown in fig. 3. The profiles of the blades of the head-cutter used for the generation of the pinion are shown in fig. 16.

The derivation of the equations of the pinion tooth surface generated by a head-cutter with circular arc blades is based on the following procedure:

Step 1:

The coordinates of the center of the blade circular arc for the concave side are represented by the following equations (fig. 16) :

$$\overline{O_oC_1} = \overline{OM_1} + \overline{M_1C_1} \tag{48}$$

where $\overline{OM_1} = r_{c_1}$, $\overline{M_1C_1} = R_1$

Equation (48) yields the following equations for the coordinates of center C_1

$$\left.\begin{array}{ll} x_o^{(C_1)} & = \overline{O_oC_1} \cdot \mathbf{i}_o = r_{c_1} - R_1 \cos\alpha_p \\ y_o^{(C_1)} & = \overline{O_oC_1} \cdot \mathbf{j}_o = 0 \\ z_o^{(C_1)} & = \overline{O_oC_1} \cdot \mathbf{k}_o = -R_1 \sin\alpha_p \end{array}\right\} \tag{49}$$

Step 2:

The position vector of a current point of the circular arc is represented in S_o by the equation (fig.16)

$$\overline{O_oA} = \overline{O_oC_1} + \overline{C_1A} = \overline{O_oC_1} + R_1\mathbf{n}_o \tag{50}$$

where

$$\mathbf{n}_o = [\cos\lambda_1 \quad 0 \quad -\sin\lambda_1]^T \tag{51}$$

is the unit normal to the circular arc that is represented in S_o.

Step 3:

The head-cutter surface is a surface of revolution that is generated while the circular arc is rotated about the axis of the head cutter. The head-cutter surface is represented in coordinate system S_{p_1} as follows

$$\mathbf{r}_{p_1} = \mathbf{r}_{p_1}^{(C_1)} + R_1\mathbf{n}_{p_1} \tag{52}$$

Here

$$\mathbf{r}_{p_1}^{(C_1)} = \mathbf{L}_{p_1 o}\mathbf{r}_o^{(C_1)} \tag{53}$$

is the position vector of point C_1 that is represented in S_1

$$\mathbf{n}_{p_1} = \mathbf{L}_{p_1 o}\mathbf{n}_o \tag{54}$$

is the unit normal to the generating surface that is represented in S_{p_1}

$$\mathbf{L}_{p_1 o} = \begin{bmatrix} \cos\theta_p & -\sin\theta_p & 0 \\ \sin\theta_p & \cos\theta_p & 0 \\ 0 & 0 & 1 \end{bmatrix} \tag{55}$$

Step 4:

For the following derivations, we represent the surface of the head-cutter in coordinate system S_m (fig. 10(b)). We may use for this purpose the following vector equation

$$\mathbf{r}_m = \overrightarrow{O_{c_1}O_{p_1}} + \mathbf{r}_m^{(C_1)} + R_1\mathbf{n}_m \tag{56}$$

Here (fig. 10(b))

$$\overline{O_{c_1}O_{p_1}} = S_{r1}[\cos q_1 \quad \sin q_1 \quad 0]^T \tag{57}$$

$$\mathbf{r}_m^{(C_1)} = \mathbf{L}_{mC_1}\mathbf{r}_{p_1} \tag{58}$$

$$\mathbf{n}_m = \mathbf{L}_{mC_1}\mathbf{n}_{p_1} \tag{59}$$

$$\mathbf{L}_{mC_1} = \begin{bmatrix} \cos\phi_c & -\sin\phi_c & 0 \\ \sin\phi_c & \cos\phi_c & 0 \\ 0 & 0 & 1 \end{bmatrix} \tag{60}$$

Step 5:

The pinion tooth surface is represented in S_1 as the envelope to the family of the head-cutter surfaces that is generated in coordinate system S_1. The equation of the family of surfaces is as follows :

$$\mathbf{r}_1(\lambda_1, \theta_p, \phi_{c_1}) = \mathbf{M}_{1d}(\phi_1)\mathbf{M}_{d_1m}\mathbf{r}_m(\lambda_1, \theta_p, \phi_{c_1}) \tag{61}$$

As a reminder, angles ϕ_{c_1} and ϕ_1, angles of rotation of the cradle and the pinion, are related by the equation

$$\phi_{c_1} = \phi_1 \sin\gamma_1 \tag{62}$$

Step 6:

The envelope to the family of surfaces is determined by equation (61) and the equation of meshing that we represent as follows

$$\mathbf{v}_m^{(1p_1)} \cdot \mathbf{n}_m = 0 \tag{63}$$

The final expression of the equation of meshing is based on the following derivations. The sliding velocity is determined as

$$\mathbf{v}_m^{(1p_1)} = \omega_m^{(1p_1)} \times \mathbf{r}_m = (\omega_m^{(1)} - \omega_m^{(p_1)}) \times \mathbf{M}_{mp_1}\mathbf{r}_{p_1} = \omega_m^{(1p_1)} \times (\mathbf{r}_m^{(C_1)} + R_1\mathbf{n}_m) \tag{64}$$

Equations (63) and (64) yield

$$(\omega_m^{(1p_1)} \times \mathbf{r}_m^{(C_1)}) \cdot \mathbf{n}_m = \mathbf{v}_m^{(1p_1,C_1)} \tag{65}$$

where

$$\mathbf{r}_m^{(C_1)} = \mathbf{L}_{mp_1}\mathbf{r}_{p_1} \tag{66}$$

and $\mathbf{v}_m^{(1p_1,C_1)}$ designates the relative velocity for point C_1.

Step 7:

The surface unit normal $\mathbf{n}_m$ is a vector function of three variables $(\lambda_1, \theta, \phi_c)$. We may simplify the vector function $\mathbf{n}_m(\lambda_1, \theta, \phi_c)$ using the following considerations :

(1) Equations

$$\mathbf{v}_m^{(1p_1)} \cdot \mathbf{n}_m = 0 \tag{67}$$

and

$$\mathbf{v}_m^{(1p_1,C_1)} \cdot \mathbf{n}_m = 0 \tag{68}$$

yield that the relative velocities determined at the point of tangency of the head-cutter and the pinion, and at the center of the circular arc are collinear. Taking this into account, we may represent the unit normal $\mathbf{n}_m$ to the surface of the head-cutter by the following equation

$$\mathbf{n}_m = \frac{\mathbf{r}_m \times \mathbf{v}_m^{(1p_1,C_1)}}{|\mathbf{r}_m \times \mathbf{v}_m^{(1p_1,C_1)}|} \tag{69}$$

where τ_m is a unit vector of the tangent to the θ_p coordinate line on the head-cutter surface, that is represented in S_m system. The unit vector τ_m is represented by the following equation

$$\tau_m(\theta_p) = \mathbf{L}_{mp_1}\mathbf{L}_{p_1 o}\mathbf{j}_o = \mathbf{L}_{mp_1}\tau_{p_1} \tag{70}$$

Vector $\mathbf{j}_o$ is perpendicular to the plane (x_o, z_o) of the circular arc (fig. 16). A point of the circular arc traces out in S_{p_1} a circle, and the unit tangent τ_{p_1} is represented as

$$\tau_{p_1} = \mathbf{L}_{p_1 o}\mathbf{j}_o = \begin{bmatrix} -\sin\theta_p \\ \cos\theta_p \\ 0 \end{bmatrix} \tag{71}$$

The advantage of application of equation (69) is that we may represent the surface unit normal by the vector function $\mathbf{n}_m(\theta_p, \phi_{c_1})$. Then, the equation of meshing will yield the relation

$$\mathbf{v}_m^{(1p_1,C_1)} \cdot \mathbf{n}_m = f(\theta_p, \phi_{c_1}) = 0 \tag{72}$$

that is free of parameter λ_1.

Angle λ_1 can be obtained from the equation

$$cos\lambda_1 = \tau_m \cdot \mathbf{n}_m \tag{73}$$

Note : Similarly, we may derive the equations of the convex side of the pinion tooth surface. Center C_2 of the circular arc (fig. 16) is represented in S_o by the equations

$$\left.\begin{array}{ll} x_o^{(C_2)} & = r_{c_2} + R_2\cos\alpha_p \\ y_o^{(C_2)} & = 0 \\ z_o^{(C_2)} & = -R_2\sin\alpha_p \end{array}\right\} \tag{74}$$

6 Computerized Simulation of Meshing and Contact

The goals of this investigation are : (i) the determination of paths of contact for aligned and misaligned gear drives, (ii) and the determination of influence of misalignment on the transmission errors and the shift of the bearing contact.

Conditions of Continuous Tangency

We set up three coordinate systems S_h, S_1, S_2 (fig. 17) that are rigidly connected to the frame, the pinion and the gear; ϕ_1' and ϕ_2' are the angles of rotation of the pinion and the gear when they are in mesh; H, V, Q δ' are the paran s used to simulate the misalignments that represent.

The contact of the tooth surfaces is localized and they are in tangency at every instant at a point. The simulation of meshing is based on the condition of continuous tangency of pinion-gear tooth surfaces Σ_1 and Σ_2, that are represented in coordinate system S_h as follows

$$\mathbf{r}_h^{(1)}(\theta_p, \phi_{c_1}, \phi_1') = \mathbf{r}_h^{(2)}(\theta_G, \phi_{c_2}, \phi_2') \tag{75}$$

$$\mathbf{n}_h^{(1)}(\theta_p, \phi_{c_1}, \phi_1') = \mathbf{n}_h^{(2)}(\theta_G, \phi_{c_2}, \phi_2') \tag{76}$$

where $|\mathbf{n}_h^{(1)}| = |\mathbf{n}_h^{(2)}| = 1$; (θ_p, ϕ_{c_1}),(θ_G, ϕ_{c_2}) are the surface parameters of the pinion and the gear, respectively; ϕ_1' ϕ_2' are the angles of rotation of the pinion and the gear being in mesh.

Equations (75) and (76) represent a system of five nonlinear equations in six unknowns represented as

$$f_i(\theta_p, \phi_{c_1}, \phi_1', \theta_G, \phi_{c_2}, \phi_2') = 0 \qquad (i = 1, 5) \tag{77}$$

where $f_i \in C'$

One of the unknowns in equation system (77), say ϕ_1', is chosen as the input one. The continuous solution of these equations is an iterative process that is based on the following procedure.

Using the first guess, we consider that a set of parameters designated as

$$P^{(o)} = (\theta_p^{(o)}, \phi_{c_1}^{(o)}, (\phi_1')^{(o)}, \theta_G^{(o)}, \phi_{c_2}^{(o)}, (\phi_2')^{(o)}) \tag{78}$$

satisfies equation system (77). We assume as well, that we have

$$\Delta_5 = \frac{\partial(f_1, f_2, f_3, f_4, f_5)}{\partial(\theta_p, \phi_{c_1}, \theta_G, \phi_{c_2}, \phi_2')} \neq 0 \tag{79}$$

Then, in accordance to the Theorem of Implicit Function System Existence [15], equation system (77) can be solved in the neighborhood of $P^{(o)}$ by functions

$$\theta_p(\phi_1'), \phi_{c_1}(\phi_1'), \theta_G(\phi_1'), \phi_{c_2}(\phi_1'), \phi_2'(\phi_1') \tag{80}$$

The solution of these nonlinear simultaneous equations is found by numerical methods.

The path of contact on the pinion tooth surface may be represented by the following expressions

$$r_1(\theta_p, \phi_{c_1}), \quad \theta_p(\phi_1'), \quad \phi_{c_1}(\phi_1') \tag{81}$$

Similarly, the path of contact on surface Σ_2 may be represented by

$$r_2(\theta_G, \phi_{c_2}), \quad \theta_G(\phi_1'), \quad \phi_{c_2}(\phi_1') \tag{82}$$

The transmission errors caused by misalignment are determined by the equation

$$\Delta\phi_2' = \phi_2' - \frac{N_1}{N_2}\phi_1' \tag{83}$$

Derivation of Equation System (80)

We use for derivation matrix equations (84)–(87), equations of surfaces Σ_p and Σ_G, and the surface unit normals.

$$\begin{aligned}\mathbf{r}_h^{(1)}(\theta_p, \phi_{c_1}, \phi_1') &= \mathbf{M}_{h1}(\phi_1')\mathbf{r}_1(\theta_p, \phi_{c_1}) \\ &= \begin{bmatrix} 1 & 0 & 0 & H \\ 0 & \cos\phi_1' & \sin\phi_1' & 0 \\ 0 & -\sin\phi_1' & \cos\phi_1' & 0 \\ 0 & 0 & 0 & 1 \end{bmatrix} \mathbf{r}_1(\theta_p, \phi_{c_1}) \end{aligned} \tag{84}$$

$$\begin{aligned}\mathbf{r}_h^{(2)}(\theta_G, \phi_{c_2}, \phi_2') &= \mathbf{M}_{h2}(\phi_2')\mathbf{r}_2(\theta_G, \phi_{c_2}) \\ &= \begin{bmatrix} \cos(\gamma+\delta') & 0 & -\sin(\gamma+\delta') & Q \\ 0 & 1 & 0 & -V \\ \sin(\gamma+\delta') & 0 & \cos(\gamma+\delta') & 0 \\ 0 & 0 & 0 & 1 \end{bmatrix} \begin{bmatrix} 1 & 0 & 0 & 0 \\ 0 & \cos\phi_2' & -\sin\phi_2' & 0 \\ 0 & \sin\phi_2' & \cos\phi_2' & 0 \\ 0 & 0 & 0 & 1 \end{bmatrix} \mathbf{r}_2(\theta_G, \phi_{c_2}) \end{aligned} \tag{85}$$

$$\mathbf{n}_h^{(1)}(\theta_p, \phi_{c_1}, \phi_1') = \begin{bmatrix} 1 & 0 & 0 \\ 0 & \cos\phi_1' & \sin\phi_1' \\ 0 & -\sin\phi_1' & \cos\phi_1' \end{bmatrix} \mathbf{n}_1(\theta_p, \phi_{c_1}) \tag{86}$$

$$\begin{aligned}&\mathbf{n}_h^{(2)}(\theta_G, \phi_{c_2}, \phi_2') \\ &= \begin{bmatrix} \cos(\gamma+\delta') & 0 & -\sin(\gamma+\delta') \\ 0 & 1 & 0 \\ \sin(\gamma+\delta') & 0 & \cos(\gamma+\delta') \end{bmatrix} \begin{bmatrix} 1 & 0 & 0 \\ 0 & \cos\phi_2' & -\sin\phi_2' \\ 0 & \sin\phi_2' & \cos\phi_2' \end{bmatrix} \mathbf{n}_2(\theta_G, \phi_{c_2}) \end{aligned} \tag{87}$$

Here; γ_1 is the pitch angle of the pinion, $\gamma_2 = \gamma - \gamma_1$, γ is the angle formed by the pinion-gear axes of rotation. Usually, $\gamma = 90°$.

Be advised that in the case when the generating surface is a cone, the unit normal is represented by a vector function of one variable (see Section 3)

Bearing Contact

Theoretically, the pinion and gear tooth surfaces are in point contact. Under the load, the contact is spread over an elliptical area. The determination of dimensions and orientation

of the instantaneous contact requires the knowledge of principal curvatures and directions of the contacting surfaces. The solution to this problem is substantially simplified due to representation of the curvatures of the generated surface by the curvatures of the generating surface and the parameters of motion [15].

For the case when the pinion generating surface is a cone, the principal curvatures of the pinion generating surface are represented as

$$\begin{aligned} k_1^{(1)} &= 0 \\ k_2^{(1)} &= \cos\alpha_p/(r_{cp} - S_p \sin\alpha_p) \end{aligned} \tag{88}$$

The principal directions on the pinion generating cone are

$$\begin{aligned} \mathbf{e}_1^{(1)} &= [-\sin\theta_p \quad \cos\theta_p \quad 0]^T \\ \mathbf{e}_2^{(1)} &= [\sin\alpha_p \cos\theta_p \quad \sin\alpha_p \sin\theta_p \quad -\cos\alpha_p]^T \end{aligned} \tag{89}$$

For the case when the pinion generating surface is a surface of revolution, the principal curvatures of the pinion generating surface are represented as

$$\begin{aligned} k_1^{(1)} &= 1/R_1 \\ k_2^{(1)} &= \cos\lambda_1/(X_o + R_1 \cdot \cos\lambda_1) \end{aligned} \tag{90}$$

The principal directions on the pinion generating cone are

$$\begin{aligned} \mathbf{e}_1^{(1)} &= [-\sin\theta_p \quad \cos\theta_p \quad 0]^T \\ \mathbf{e}_2^{(1)} &= [\sin\lambda_1 \cos\theta_p \quad \sin\lambda_1 \sin\theta_p \quad -\cos\lambda_1]^T \end{aligned} \tag{91}$$

Similarly, when the generating surface of the gear is also a cone, we have that the principal curvatures of the gear generating surface are

$$\begin{aligned} k_1^{(2)} &= 0 \\ k_2^{(2)} &= \cos\alpha_G/(r_c - S_G \sin\alpha_G) \end{aligned} \tag{92}$$

The principal directions on the gear generating surface are

$$\begin{aligned} \mathbf{e}_1^{(2)} &= [-\sin\theta_G \quad \cos\theta_G \quad 0]^T \\ \mathbf{e}_2^{(2)} &= [\sin\alpha_G\cos\theta_G \quad \sin\alpha_G\sin\theta_G \quad -\cos\alpha_G]^T \end{aligned} \tag{93}$$

The principal directions are represented in systems S_{p_1} for the pinion case, and S_{p_2} for the gear case, respectively.

Because the generating and generated surfaces are in line contact, their principal curvatures and directions are related by the following three equations [15]

$$\begin{aligned} \tan 2\sigma &= \frac{2t_{13}t_{23}}{t_{23}^2 - t_{13}^2 - (k_f - k_h)t_{33}} \\ k_q - k_s &= \frac{2t_{13}t_{23}}{t_{33}\sin 2\sigma} \\ k_q + k_s &= k_f + k_h + \frac{t_{13}^2 + t_{23}^2}{t_{33}^2} \end{aligned} \tag{94}$$

Here, k_f, k_h are the principal curvatures of the generating surface; k_s, k_q are the principal curvatures of the generated surface; σ is the angle between the principal directions of the generating and generated surfaces (fig. 18(a)). The expression for t_{13}, t_{23}, and t_{33} are represented in [15].

The determination of the dimensions of the contact ellipse and its orientation is based on application of following equations

$$\tan 2\tau = \frac{g_2 \sin\alpha^{(12)}}{g_1 - g_2\cos\alpha^{(12)}} \tag{95}$$

where

$$g_1 = k_1^{(1)} - k_1^{(2)}$$

$$g_2 = k_2^{(1)} - k_2^{(2)}$$

$$\alpha^{(12)} = \cos^{-1}(\mathbf{e}_1^{(1)} \cdot \mathbf{e}_1^{(2)})$$

$k_1^{(1)}$ and $k_2^{(1)}$ are the principal curvatures of the pinion surface. $k_1^{(2)}$ and $k_2^{(2)}$ are the principal curvatures of the gear surface.

The major axis and minor axis of the contact ellipse may be determined as

$$2a = 2\sqrt{\frac{\delta}{A}}, \quad 2b = 2\sqrt{\frac{\delta}{B}} \tag{96}$$

where δ is the elastic approach obtained from experimental data; A and B are determined by

$$\begin{aligned} A &= \tfrac{1}{4}[k_\Sigma^{(1)} - k_\Sigma^{(2)} - (g_1^2 - 2g_1g_2\cos 2\alpha^{(12)} + g_2^2)^{\frac{1}{2}}] \\ B &= \tfrac{1}{4}[k_\Sigma^{(1)} - k_\Sigma^{(2)} + (g_1^2 - 2g_1g_2\cos 2\alpha^{(12)} + g_2^2)^{\frac{1}{2}}] \end{aligned} \tag{97}$$

and

$$k_\Sigma^{(1)} = k_1^{(1)} + k_2^{(1)}$$

$$k_\Sigma^{(2)} = k_1^{(2)} + k_2^{(2)}$$

7 Numerical Examples

Introduction

The purpose of the numerical examples is: (i) to determine the influence of errors of alignment on the transmission errors and the shift of the bearing contact, and (ii) to prove that the predesigned parabolic function is able to absorb the transmission errors that are caused by the errors of alignment. We emphasize that the determination of transmission errors caused by misalignment is based on the following approach:

(1) We consider an imaginary process for generation when an ideal transmission function is provided. Then, using TCA, we simulate errors of alignment and determine the transmission errors that are caused by the respective error of alignment.

(2) On the second stage of investigation, we consider again the imaginary method of generation that has been provided in the previous section. We remind that this method of generation provides for each cycle of meshing a transmission function and a predesigned parabolic function as the sum of the ideal linear function and a predesigned parabolic function. Using the TCA, we consider the meshing and contact of the gear misaligned gear drive that allows to determine: (i) the resulting function of transmission errors as the sum of the predesigned parabolic function and the function of errors that is caused by misalignment. We are also able to determine the shift of the bearing contact caused by misalignment by applying the TCA method.

The simulation of meshing and contact has been accomplished for both methods of generation described above that provide the longitudinal bearing contact, and the across the surface bearing contact. The results of computation confirmed that the bearing contact is stable, and the predesigned parabolic function is able indeed to absorb the almost linear functions of transmission errors caused by the respective errors of alignment.

Input Data:

The input data is represented in Tables 1-5.

Output Data:

The results of computation are represented for two cases of generation: (i) by application of a pinion head-cutter with straight blades (figs. 19-42); (ii) by application of a pinion head-cutter with circular arc blades (figs. 43-66). It is assumed that in both cases the gear is generated by a head-cutter with straight blades. In each case, four sets of figures represent the respective influence of H, Q, V, δ', which indicate the axial displacement of the pinion, the gear, the offset, and the change of the shaft angle, respectively. Alignment errors are given in millimeters, δ' is given in arc minutes.

Table 1: Blank Data

	Pinion	Gear
Number of teeth	11	41
Shaft angle	90°	
Mean spiral angle	35°	35°
Hand of spiral	LF	RH
Outer cone distance (mm)		90.07
Face width (mm)		27.03
Whole depth (mm)	10.0	10.0
Pitch angle	15°1′	74°59′
Root angle	15°1′	74°59′
Face angle	15°1′	74°59′

In each set of figures, we represent:

(i) The initial influence of misalignment on the transmission errors, when the predesigned parabolic function has not been applied. The transmission function caused by misalignment is almost a linear function (see. for instance, figs. 19 and 20).

(ii) The interaction of the linear function of transmission errors with the predesigned parabolic function. The results of TCA show that the obtained resulting function is indeed a parabolic function (see, for instance, figs. 21 and 23).

(iii) The location of bearing contact for a misaligned gear drive (see, for instance, figs. 23 and 24).

Similar sets of figures are represented for other kinds of misalignment.

Table 2: Gear Cutter Specification

Blade angle	20°
Cutter diameter (mm)	152.4
Point width (mm)	2.79

Table 3: Gear Machine Tool Settings

Radial setting (mm)	70.53744
Cradle angle	−62°14′
Machine center to back (mm)	0
Sliding base (mm)	0
Blank offset (mm)	0
Machine root angle	74°59′

Table 4: Pinion Machine Tool Settings for Generation by a Cone

	Convex	Concave
Cutter blade angle	20°	20°
Cutter point radius (mm)	71.7222	80.4876
Radial setting (mm)	68.04991	73.31925
Cradle angle	−57°50′	−66°12′
Machine center to back (mm)	0	0
Sliding base (mm)	0	0
Blank offset (mm)	0	0
Machine root angle	15°1′	15°1′

Table 5: Pinion Machine Tool Settings for Generation by Head-Cutter with circular Arc Blades

	Convex	Concave
Cutter point radius (mm)	71.7222	80.4876
Radial setting (mm)	68.04991	73.31925
Cradle angle	$-57°50'$	$-66°12'$
Machine center to back (mm)	0	0
Sliding base (mm)	0	0
Blank offset (mm)	0	0
Machine root angle	$15°1'$	$15°1'$

8 Conclusion

Extension of application of a CNC machine for generation of spiral bevel gears with the following features has been discussed: (i) The gears are face-milled, the tooth depth is uniform. (ii) Two types of bearing contact are provided directed (a) in the longitudinal direction, and (b) in the direction across the surface. (iii) A predesigned parabolic function of transmission errors is provided for the absorption of transmission errors caused by misalignment. (iv) Equations of generated pinion-gear tooth surfaces have been derived. (v) TCA computer program has been developed and the influence of misalignment on the transmission errors and the shift of the bearing contact has been investigated. The computations that were performed confirmed the stability of the bearing contact, the low level of transmission errors and the favorable shape of the function of transmission errors, of a parabolic type, for a misaligned gear drive.

9 Directions for TCA Program Use

There are two TCA programs for two different cases. One program is BEVEL.FOR, for the case that both the pinion and the gear generating surfaces are cone surfaces. The other program is RBEVEL.FOR, for the case that the pinion generating surface is a surface of revolution, the gear generating surface is a cone surface. For both programs the input data files and the output data files are almost the same, except that there is an additional arc radius, RHO, in the input data files for program RBEVEL.FOR.

Input data

1. Control codes

(a) For right hand gear JCH=1, for left hand gear JCH=2

(b) TL1 and TL2 are numbers of extra point on the contact path which should not be larger that 2

(c) MM is the number of contact points

2. Blank data

TN1—Pinion number of teeth

TN2—Gear number of teeth

C—Shaft offset (zero for spiral bevel gear) (mm)

TW—Face width of gear (mm)

GAMMA—Shaft angle (degree)

MCD—Mean cone distance (mm)

RGMA1—Pinion root cone angle (degree)

B1—Pinion spiral angle (degree)

B2—Gear spiral angle (degree)

RGMA2—Gear root cone angle (degree)

FGMA2—Gear face cone angle (degree)

PGMA2—Gear pitch cone angle (degree)

ADD2—Gear mean addendum (mm)

DED2—Gear mean dedendum (mm)

WD—Whole depth (mm)

CC—Clearance (mm)

DEL—Elastic approach (mm)

3. Gear cutter specification

RU2—Gear nominal cutter radius (mm)

PW2—Point width of gear cutter (mm)

ALP2—Blade angle of gear cutter (degree)

4. Gear machine-tool settings

XG2—Machine center to back (mm)

GAMA2—Gear machine root angle (degree)

XB2—Sliding base (mm)

EM2—Blank offset (mm)

4. Pinion machine-tool settings

RCF—Point radius (mm)

XG1—Machine center to back (mm)

XB1—Sliding base (mm)

EM1—Blank offset (mm)

GAMA1—Pinion machine root angle (degree)

AlP1—Blade angle of pinion cutter (degree)

6. Misalignments

A—Constant coefficient of the predesigned parabolic function

H—Misalignment along the pinion axis (mm)

Q—Misalignment along the gear axis (mm)

V—Misalignment of axis offset (mm)

δ'—Misalignment of shaft angle (arc min.)

Input data files

Files 70 and 60 are for program RBEVEL.FOR, file 70 for the convex side, file 60 for the concave side. These two files must be read together. Files 90 and 80 are for program BEVEL.FOR, file 90 for the convex side, file 80 for the concave side. These two files must be read together.

Output data files

File 9 is an overall output data file. All the input and output information is stored in this file. File 91 stores the information of transmission errors for the convex side; file 93 stores the information of transmission errors for the concave side. File 92 stores the information of contact path and contact ellipse for the convex side; file 94 stores the information of contact path and contact ellipse for the concave side.

References

(1) Baxter, M.L. 1961. Basic geometry and tooth contact of hypoid gears. Indus. Math. pp. 1-28

(2) Baxter, M.L. 1973. Second-Order Surface Generation. J. Industrial Mathematics, Vol 23, part 2, pp. 85-106

(3) Dongarrd, J.J., Bunch, J.R., Moler, C.B., and Steward, G.W. 1979. LINPACK User's Guide, SIAM, Philadelphia

(4) Dudley, D.W. 1962. Gear Handbook, The Design, Manufacture, and Application of Gears. McGraw-Hill, NY.

(5) Favard, J. Course of Local Differential Geometry, Gauthier-Villars, Paris (in French, translated into Russian)

(6) Goldrich, R.N. 1989. Theory of 6-axis generation of spiral bevel and hypoid gears. AGMA paper 89FTM9

(7) Korn, G.A. and Korn, T.M. 1968. Mathematics handbook for scientists and Engineers, 2nd ed., McGraw-Hill, NY.

(8) Litvin, F.L. 1960, 1968. Theory of Gearing, 1st ed. (1960), 2nd ed. (1968). Nauka (in Russian)

(9) Litvin, F.L. 1969. Die Beziehungen Zwischen den Krümmungen der Zahnoberflächen bei Räumlichen Verzahnungen. Z. Angew. Math. Mech. 49: 685-690 (in German)

(10) Litvin, F.L. and Gutman, Y. I. 1981. Methods of Synthesis for Hypoid Gear Drives of Formate and Helixform, ASME J. Mechan. Design. Vol. 103, pp. 83-103

(11) Litvin, F.L. Pahman P. and Goldrich R.N. 1982, Mathematical Models for the Synthesis and Optimization of Spiral Bevel Gear Tooth Surfaces, NASA CR-3553

(12) Litvin, F.L. and Zhang, Y. 1991(b). Local synthesis and tooth contact analysis of face-milled spiral bevel gears. NASA Contractor Report 4342, AVSCOM Technical Report 90-C-028

(13) Litvin, F.L. and Hsiao, C.-L. 1993. Computerized simulation of meshing and contact of enveloping gear tooth surfaces. J. Comp. Meth. Appl. Mech. Engrg. 102: 337-336

(14) Litvin, F.L. 1989. Theory of Gearing, NASA Reference Publication 1212

(15) Litvin, F.L. 1994. Gear Geometry and Applied Theory, Prentice Hall

(16) More, Jorge J., Garbow, Burton S., and Hilstorm, Kenneth E. 1980. User Guide for MINPACK-1, Argonne National Laboratory, Argonne, IL.

(17) Stadtfeld, H.J. 1993. Handbook of Bevel and Hypoid Gears. Rochester Institute of Technology

(18) Stoker, J.J. 1969. Differential Geometry, Willey-Interscience

(19) Townsend, P.S. 1991. Dudley's Gear Handbook, 2nd ed., McGraw-Hill, NY

(20) Wildhaber, E. 1946(c). Tooth Contact, Amer. Mach. 90: 110-114

(21) Wildhaber, E. 1956. Surface Curvature. Prod. Engrg. 27: 184-191

(22) Zalgaller, V.A. 1975. Theory of Envelopes, Nauka, Moscow (in Russian)

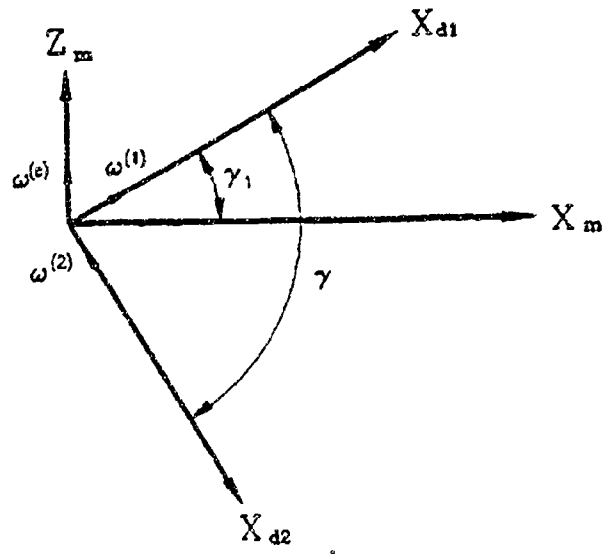

Figure 1: Representation of axes of rotation of spiral bevel gears in coordinate system S_m

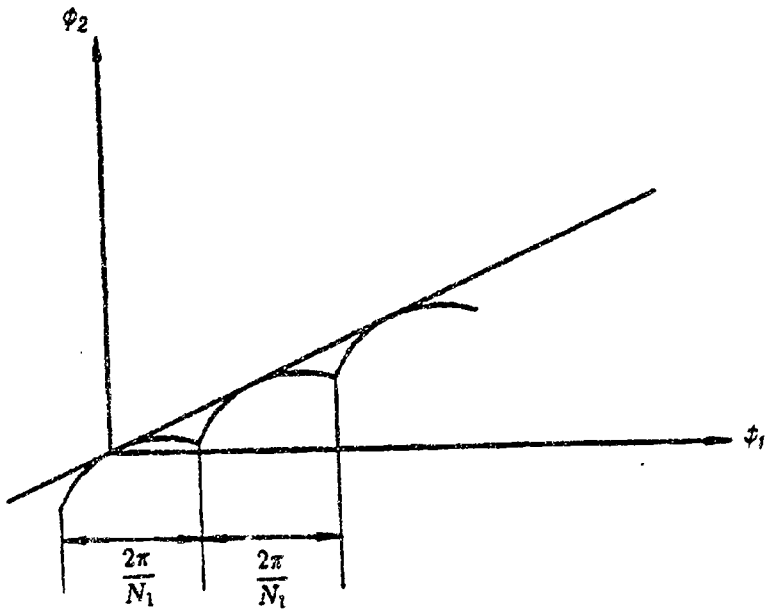

Figure 2: Transmission function $\phi_2(\phi_1)$ with a parabolic function of transmission errors

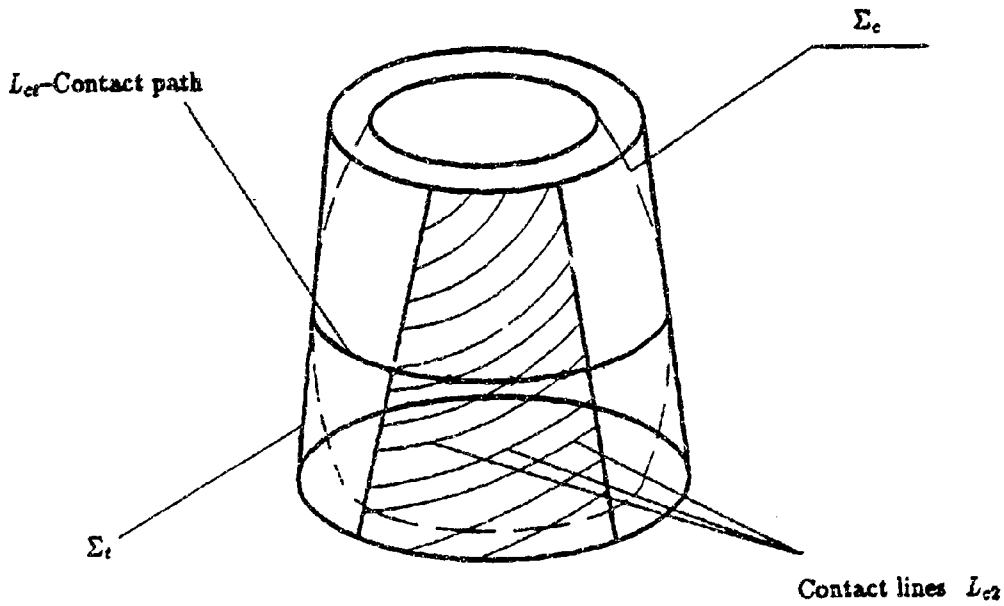

Figure 3: Generating surfaces Σ_c and Σ_t that provide contact path along the surface

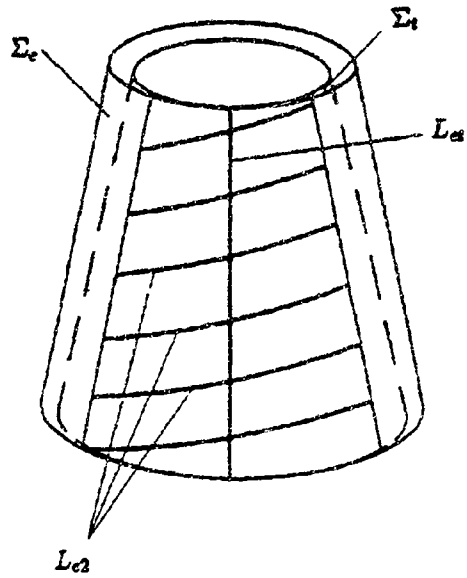

Figure 4: Generating surfaces Σ_c and Σ_t that provide a contact path across the surface

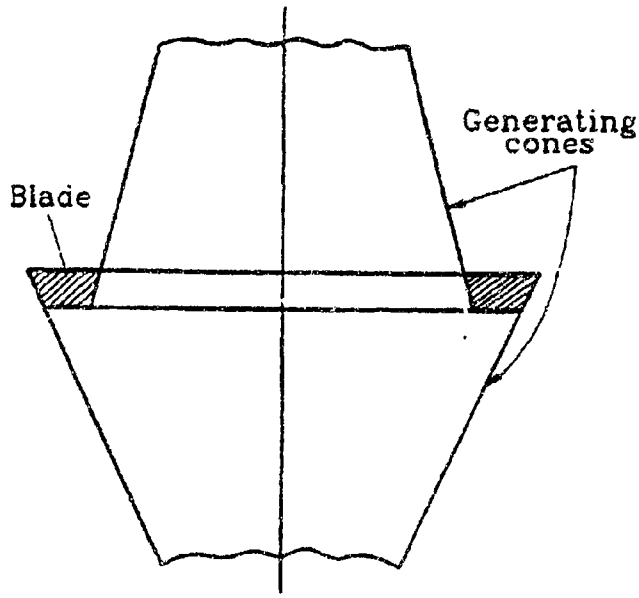

Figure 5: Generating blades and cones

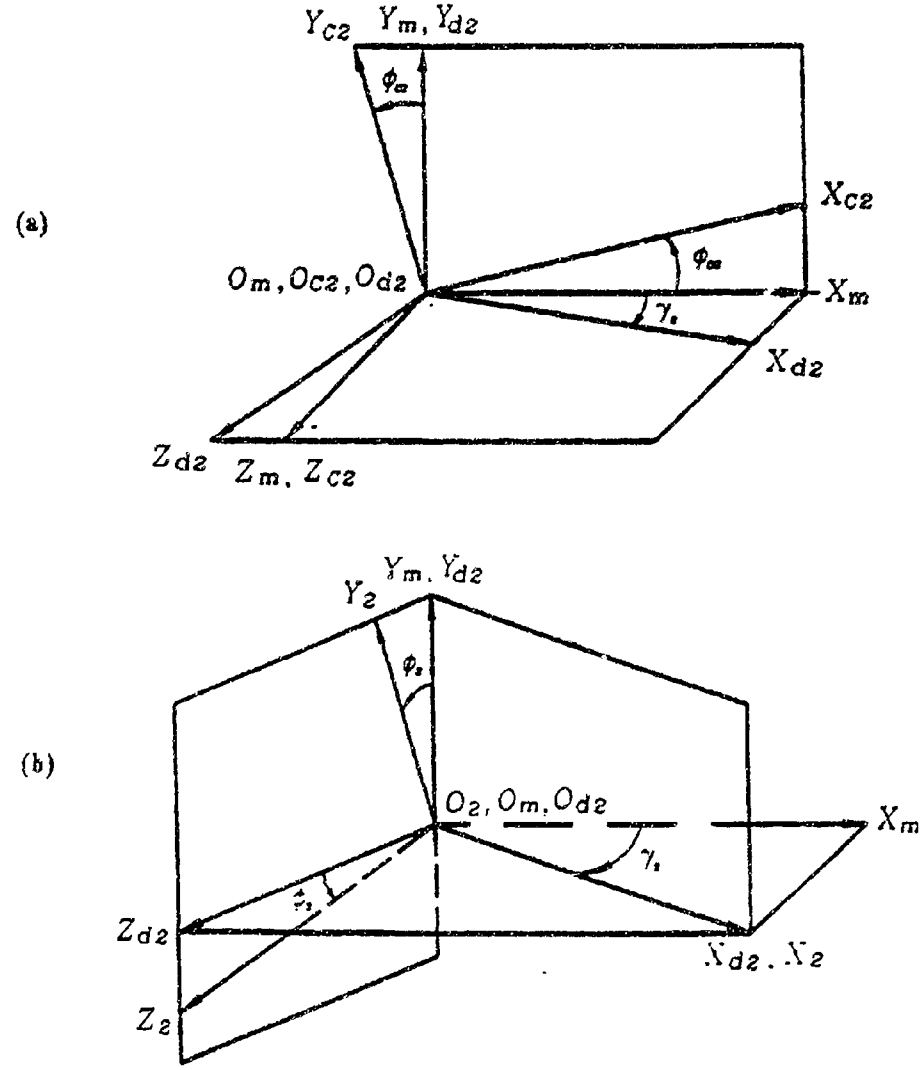

Figure 6: Installment and orientation of coordinate systems S_m, S_{c2}, S_{d2}, and S_2

(a)

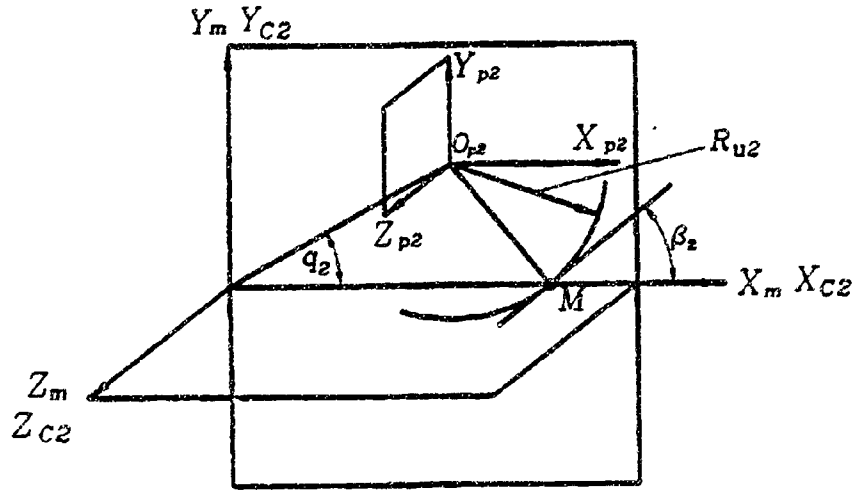

(b)

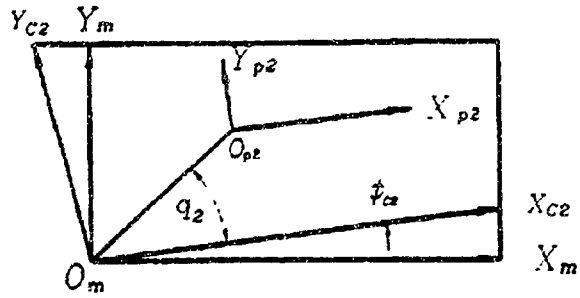

Figure 7: Coordinate systems S_m, S_{c2}, and S_{p2} applied for gear generation

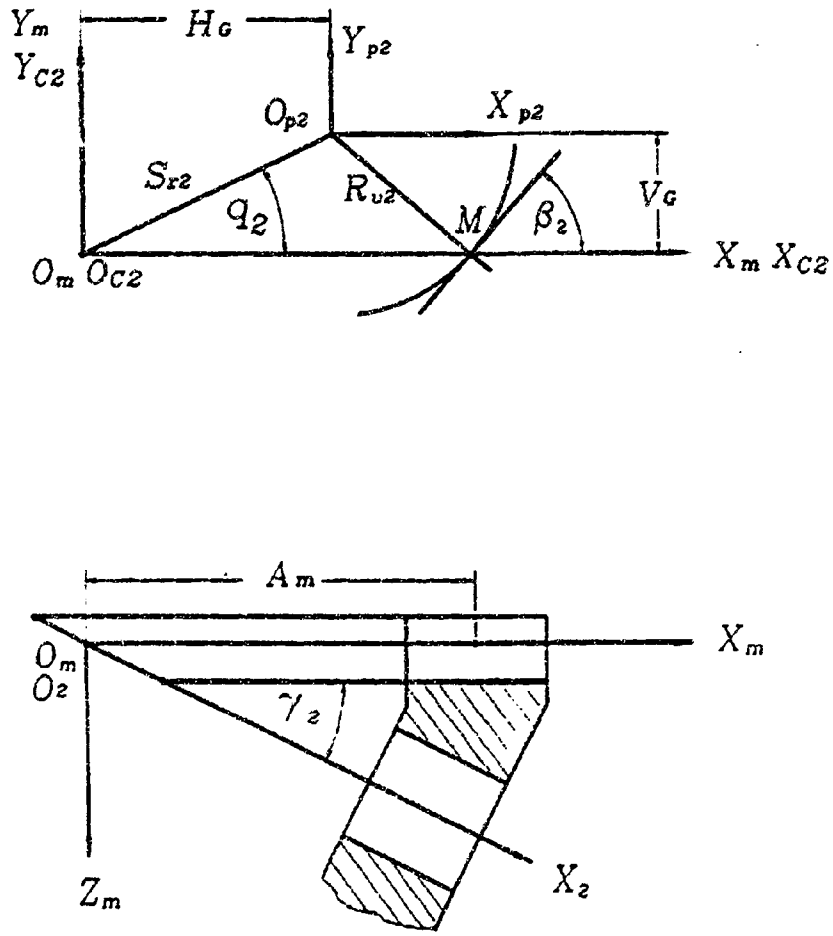

Figure 8: Machine-tool settings for gear generation

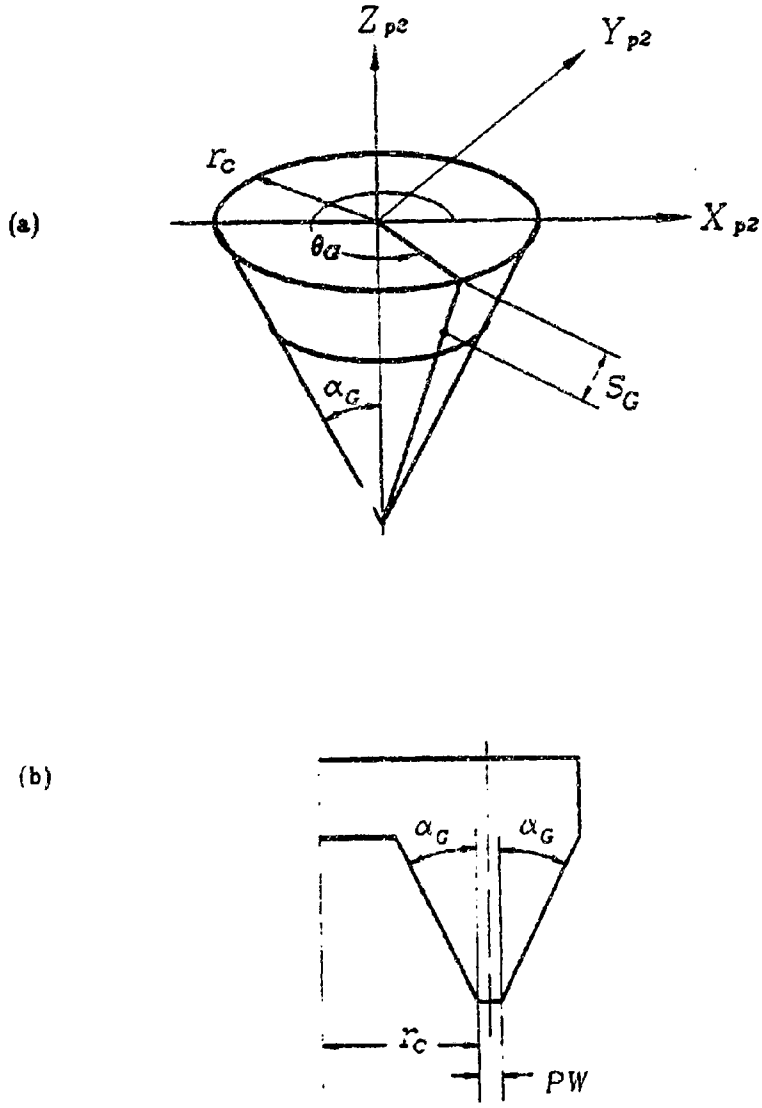

Figure 9: Gear generating surface and its straight line blade profiles

(a)

(b)

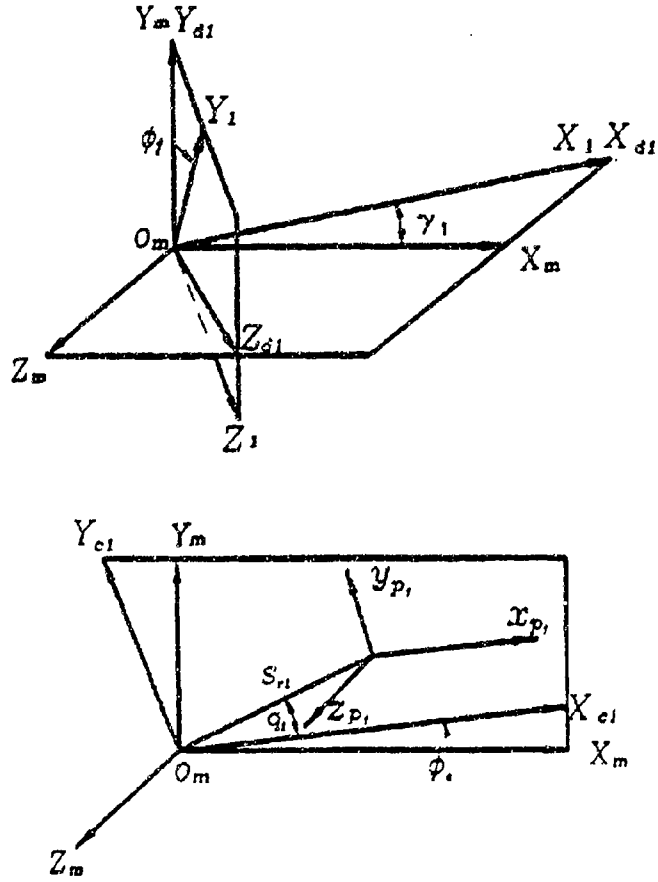

Figure 10: Coordinate systems S_m, S_{p_1}, S_{d_1} and S_{c_1} applied for pinion generation

(a)

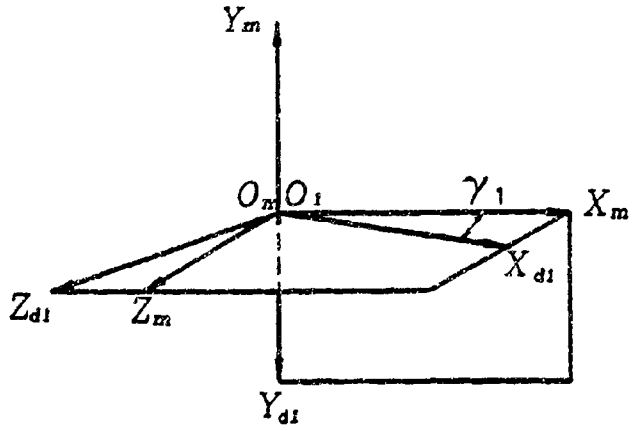

(b)

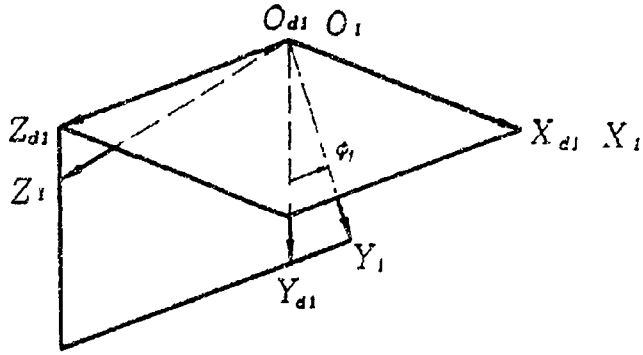

Figure 11: Coordinate systems S_m, S_{d_1} and S_1 applied for pinion generation

(a)

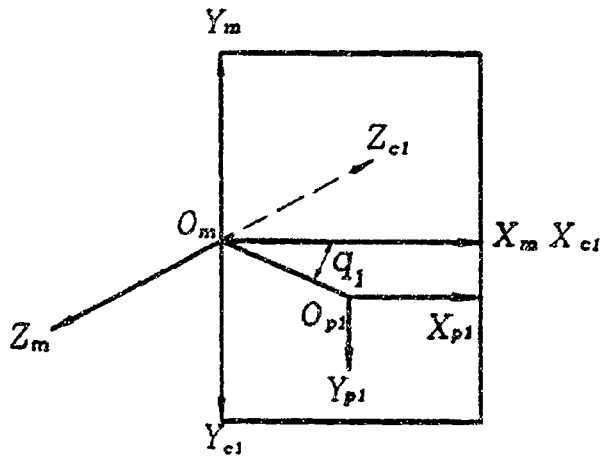

(b)

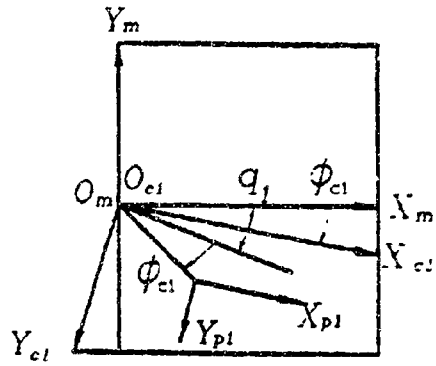

Figure 12: For derivation of relation between imaginary and real pinion machine-tool settings

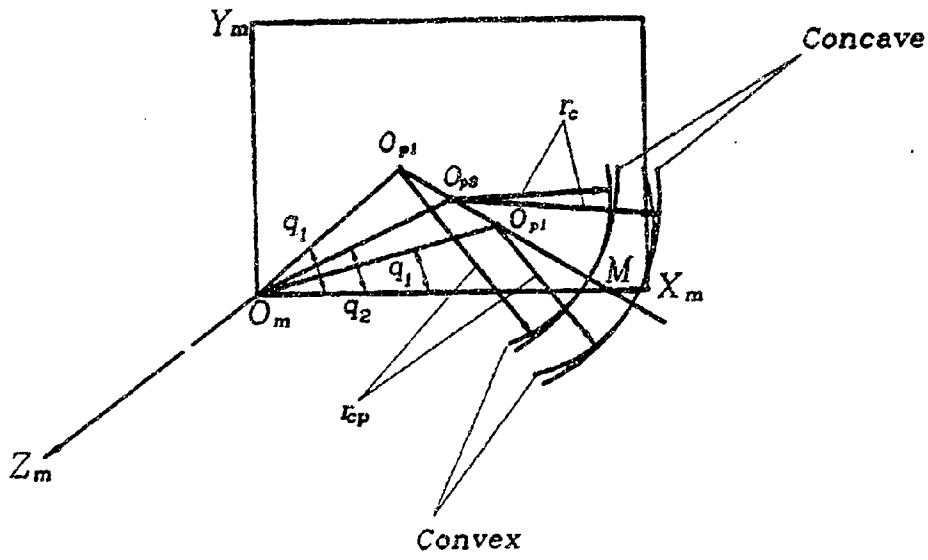

Figure 13: Profiles of pinion and gear head-cutters represented in plane $Z_m = 0$

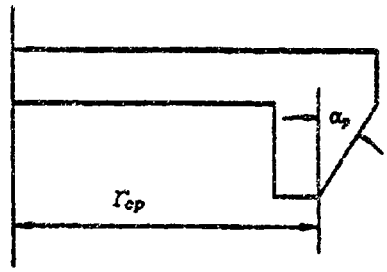

(a) For concave side

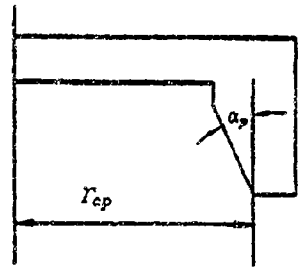

(b) For convex side

Figure 14: Profiles of straight-line pinion blades

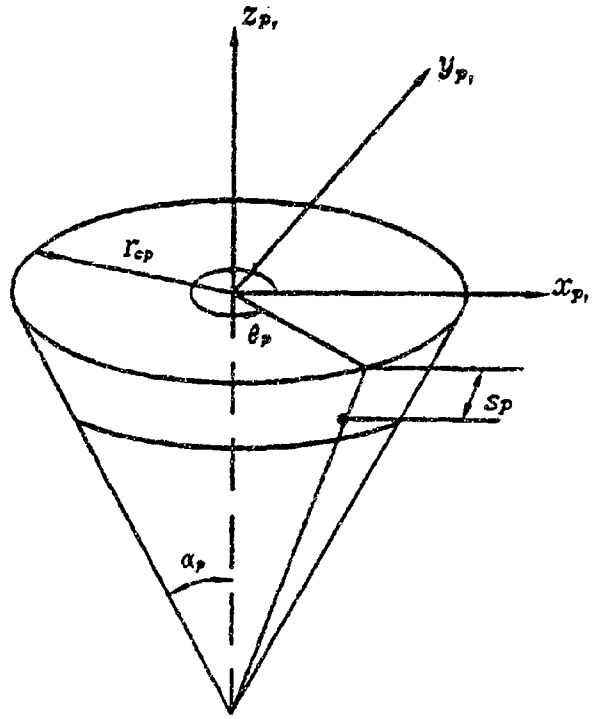

Figure 15: For derivation of pinion generating cone surface

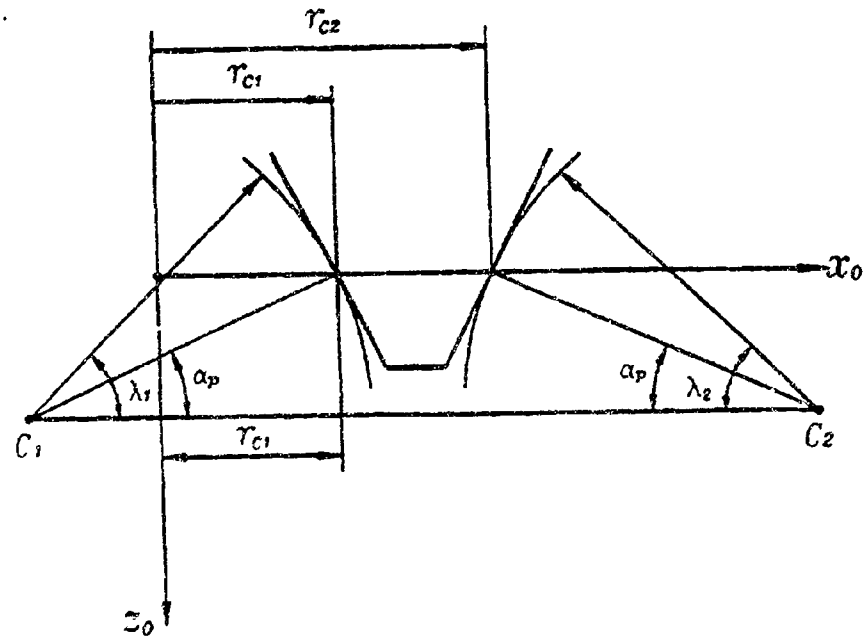

Figure 16: Profiles of pinion circular-arc blades

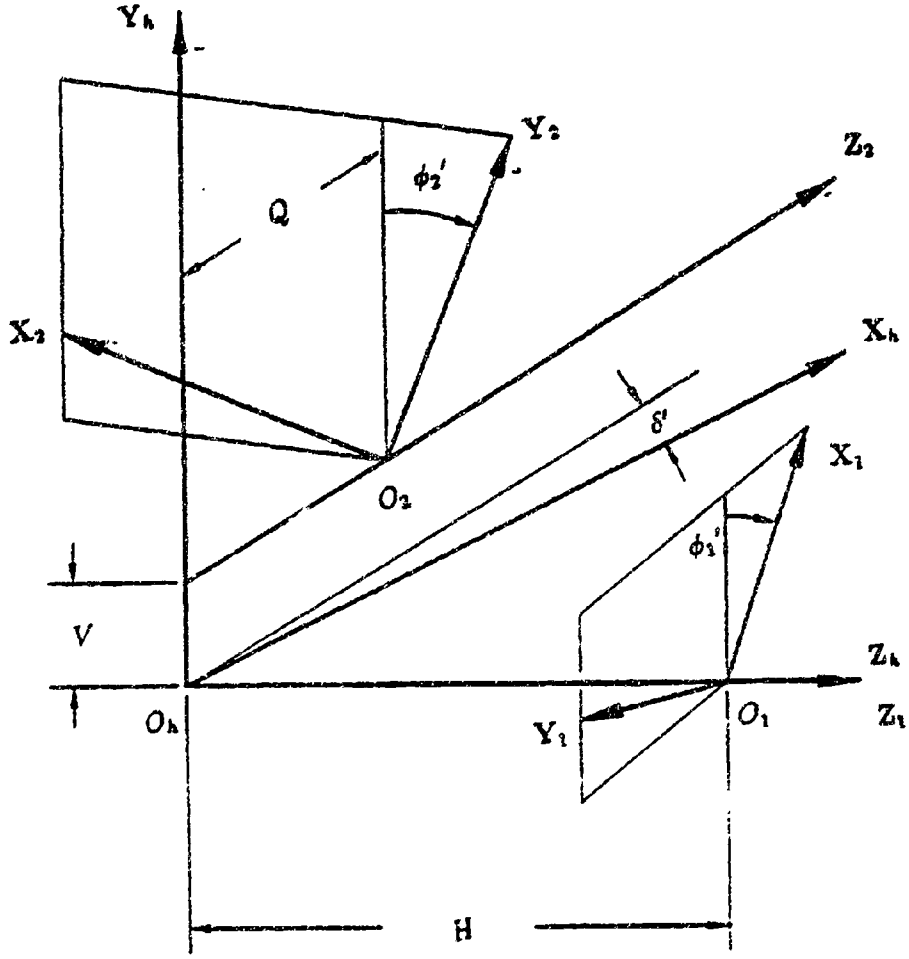

Figure 17: Coordinate systems applied for simulation of meshing

(a)

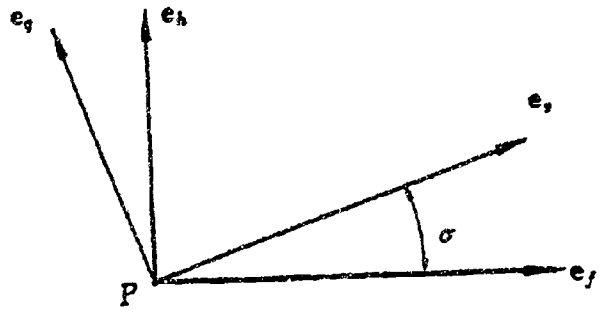

(b)

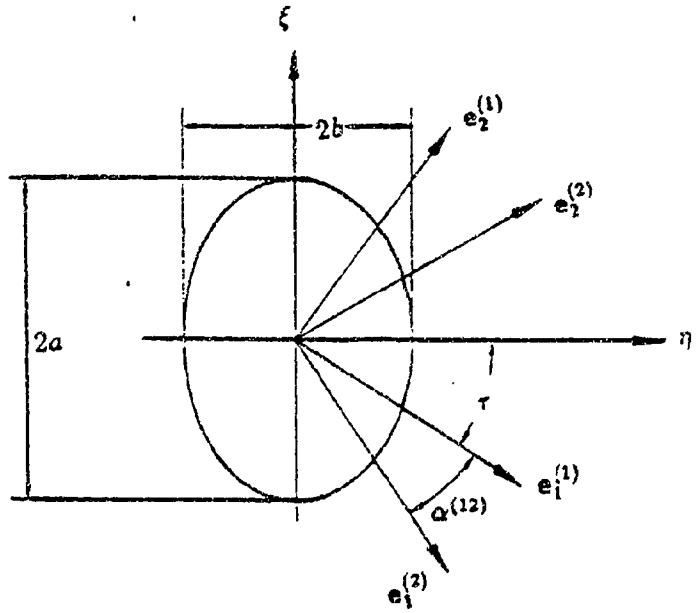

Figure 18: Principal directions and contact ellipse

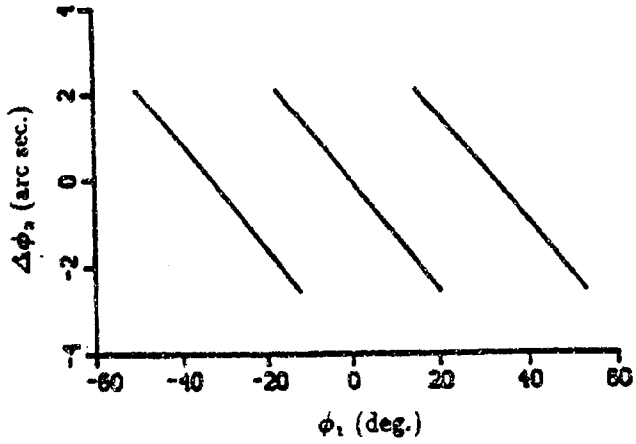

Figure 19: Transmission errors: H=0.01mm (Convex side)

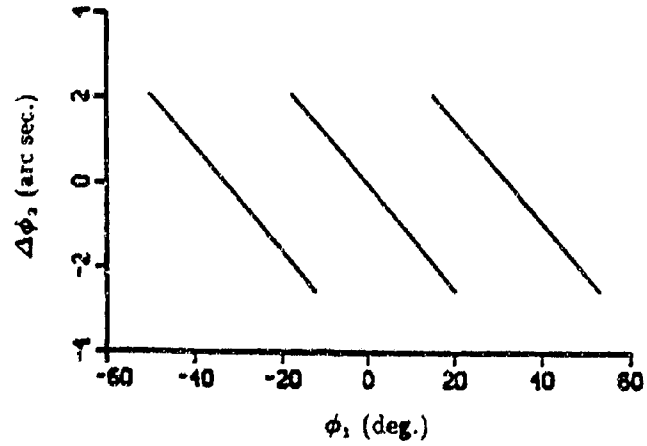

Figure 20: Transmission errors: H=0.01mm (Concave side)

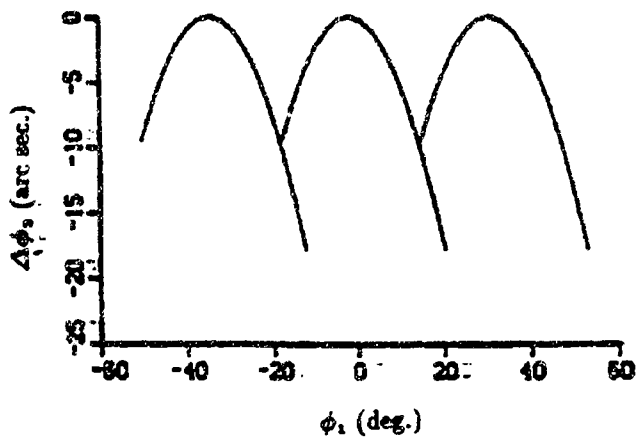

Figure 21: Resulting transmission errors: H=0.01mm (Convex side)

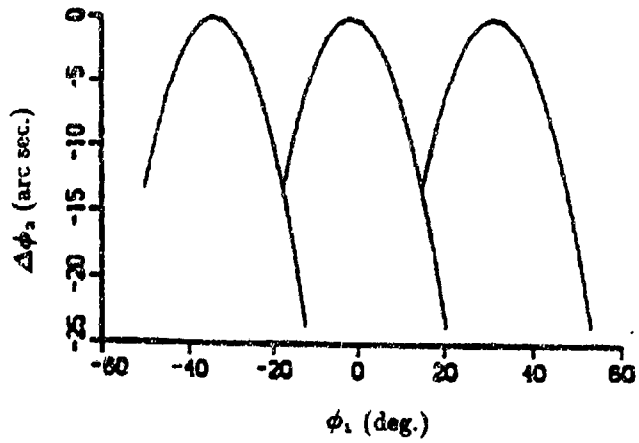

Figure 22: Resulting transmission errors: H=0.01mm (Concave side)

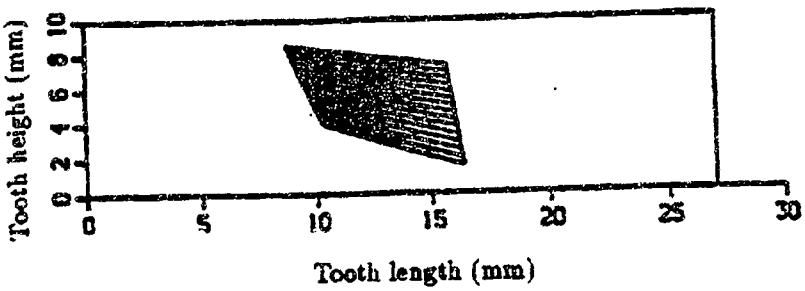

Figure 23: Shift of bearing contact: H=0.01mm (Convex side)

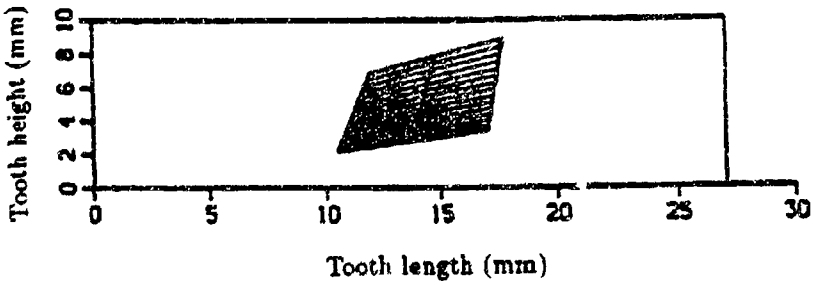

Figure 24: Shift of bearing contact: H=0.01mm (Concave side)

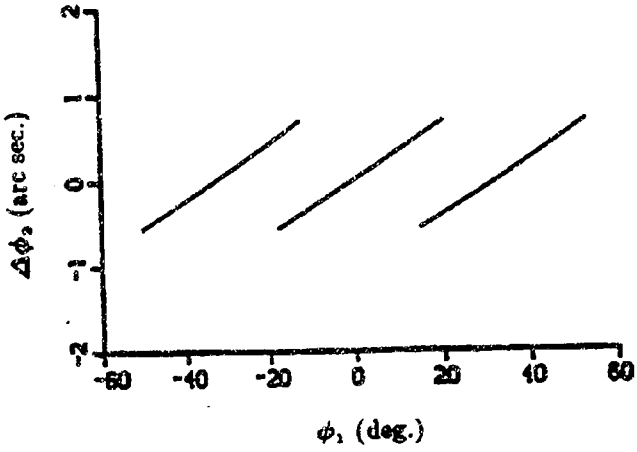

Figure 25: Transmission errors: Q=0.01mm (Convex side)

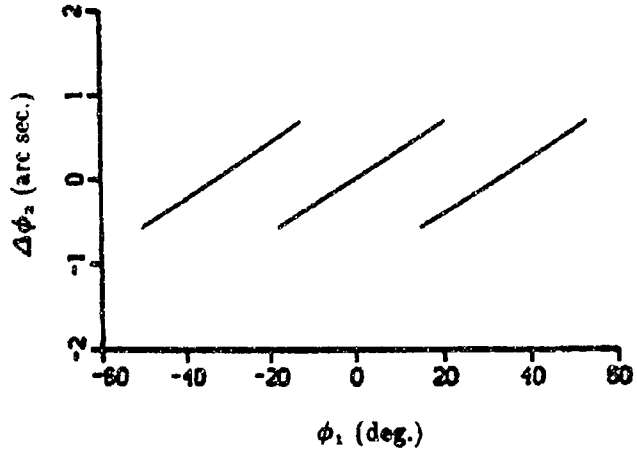

Figure 26: Transmission errors: Q=0.01mm (Concave side)

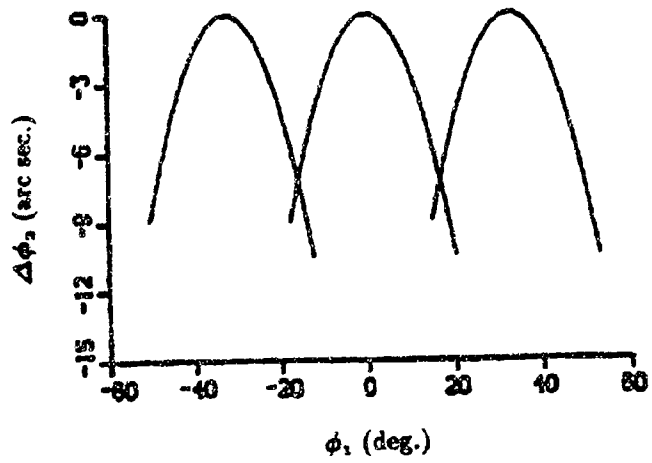

Figure 27: Resulting transmission errors: Q=0.01mm (Convex side)

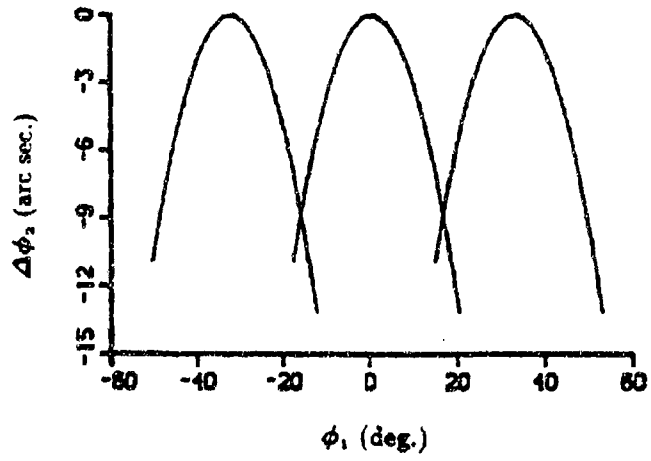

Figure 28: Resulting transmission errors: Q=0.01mm (Concave side)

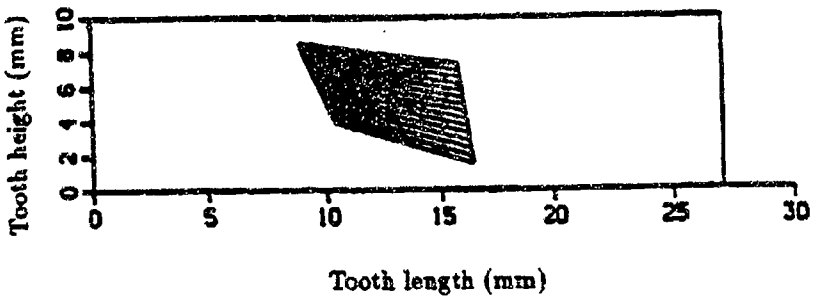

Figure 29: Shift of bearing contact: Q=0.01mm (Convex side)

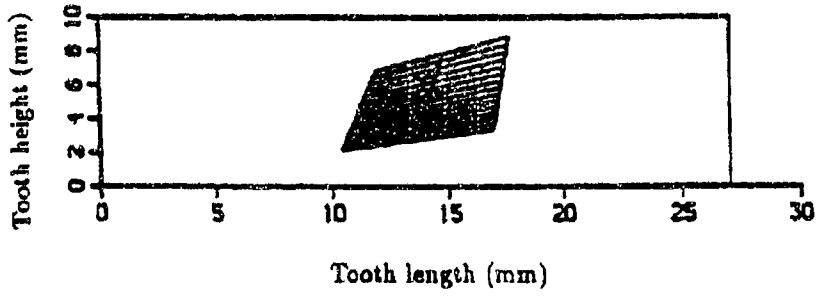

Figure 30: Shift of bearing contact: Q=0.01mm (Concave side)

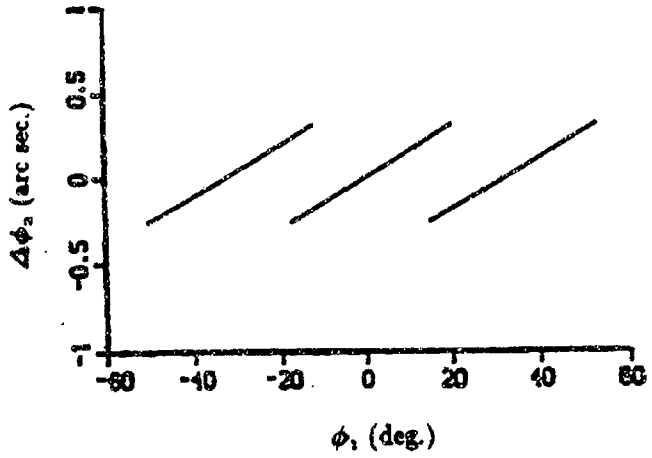

Figure 31: Transmission errors: V=0.01mm (Convex side)

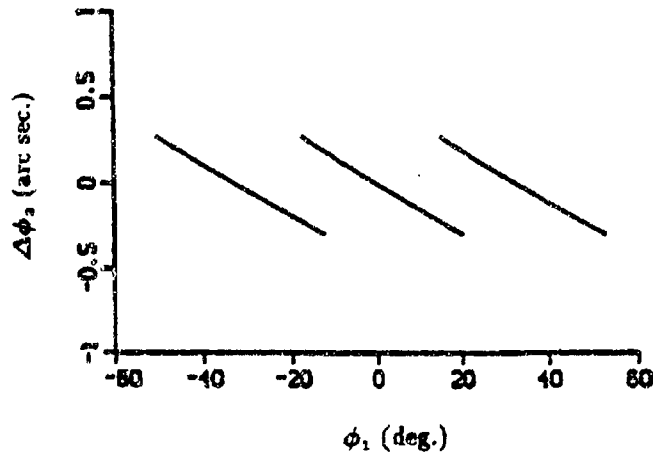

Figure 32: Transmission errors: V=0.01mm (Concave side)

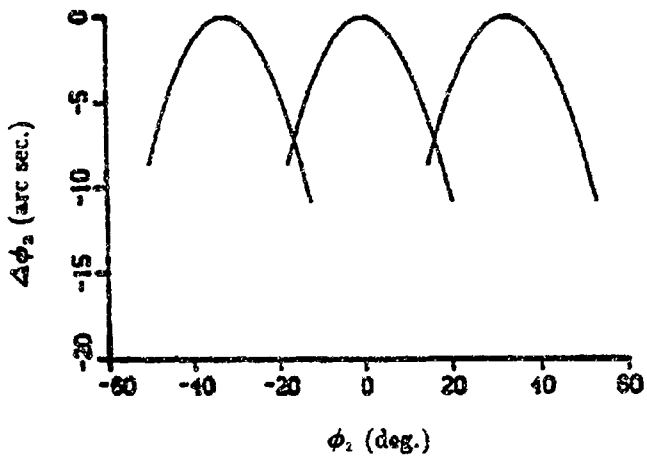

Figure 33: Resulting transmission errors: V=0.01mm (Convex side)

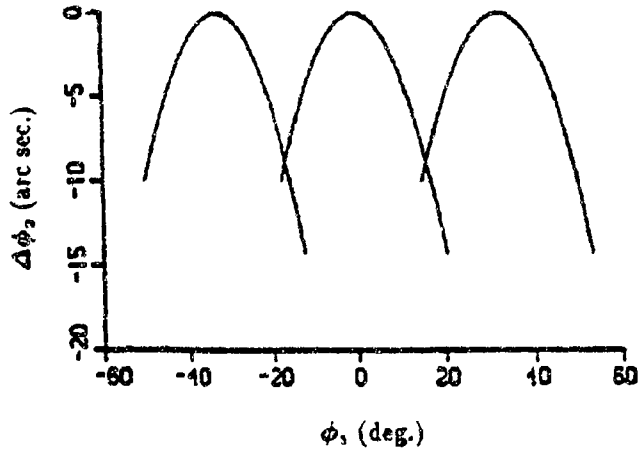

Figure 34: Resulting transmission errors: V=0.01mm (Concave side)

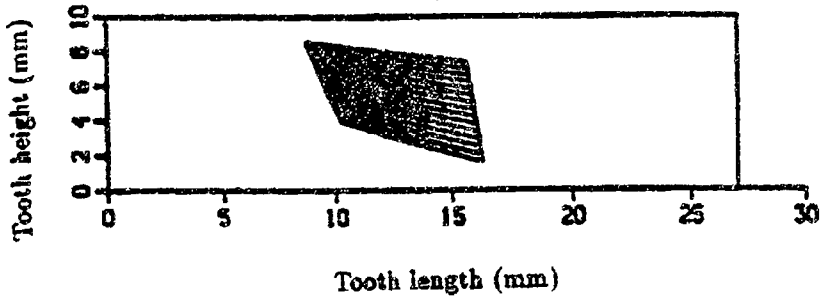

Figure 35: Shift of bearing contact: V=0.01mm (Convex side)

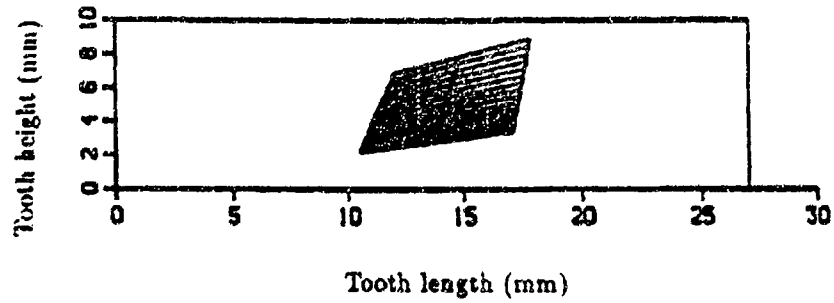

Figure 36: Shift of bearing contact: V=0.01mm (Concave side)

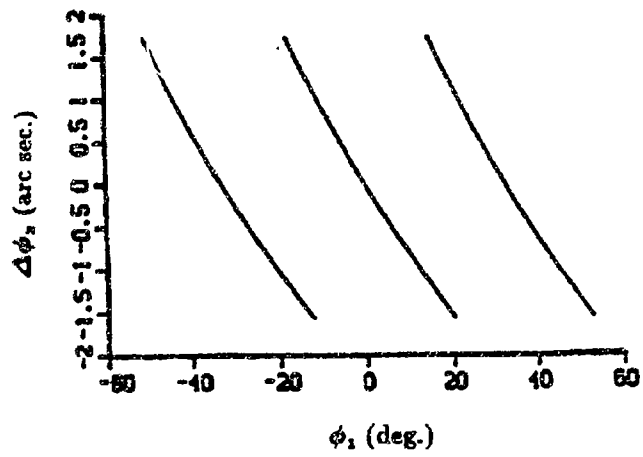

Figure 37: Transmission errors:δ'=1 arc min. (Convex side)

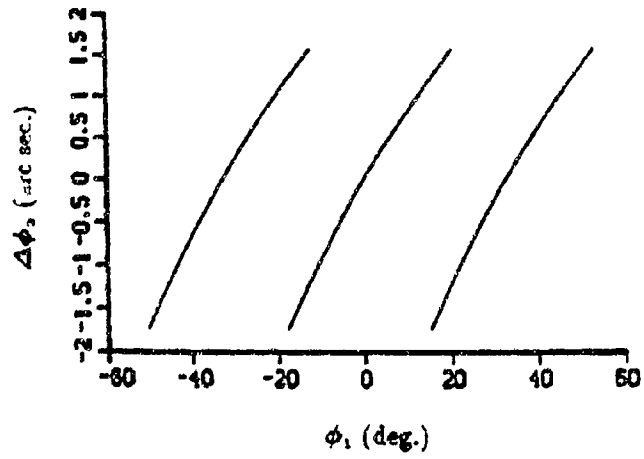

Figure 38: Transmission errors: δ'=1 arc min. (Concave side)

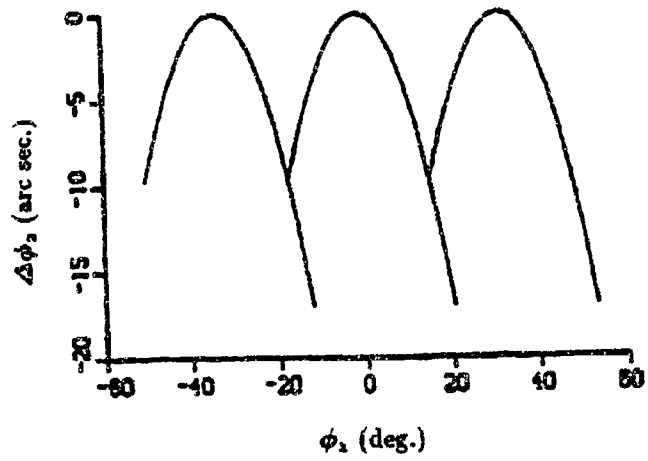

Figure 39: Resulting transmission errors: δ'=1 arc min. (Convex side)

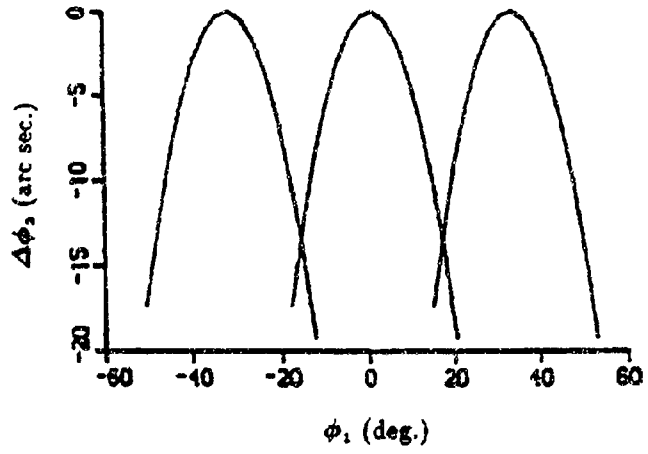

Figure 40: Resulting transmission errors: δ'=1 arc min. (Concave side)

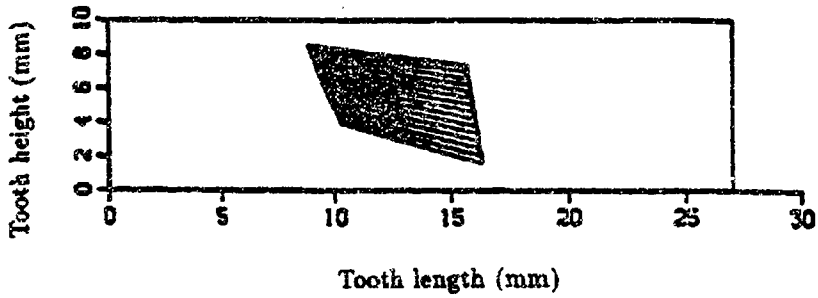

Figure 41: Shift of bearing contact: δ'=1 arc min. (Convex side)

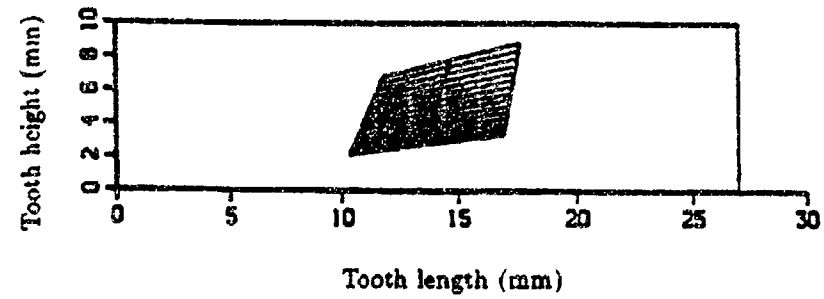

Figure 42: Shift of bearing contact: δ'=1 arc min. (Concave side)

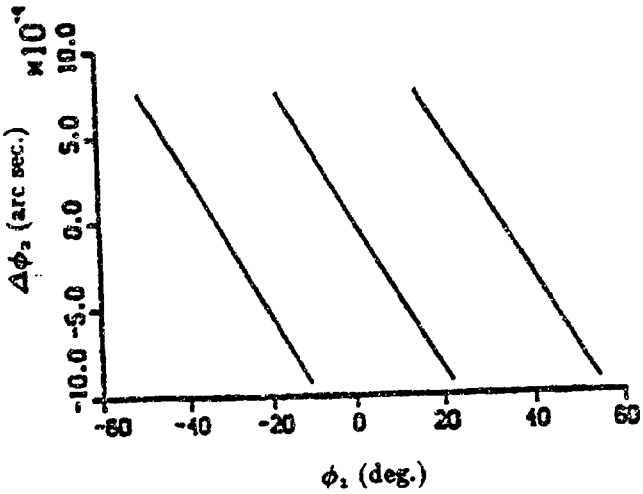

Figure 43: Transmission errors: H=0.01mm (Convex side)

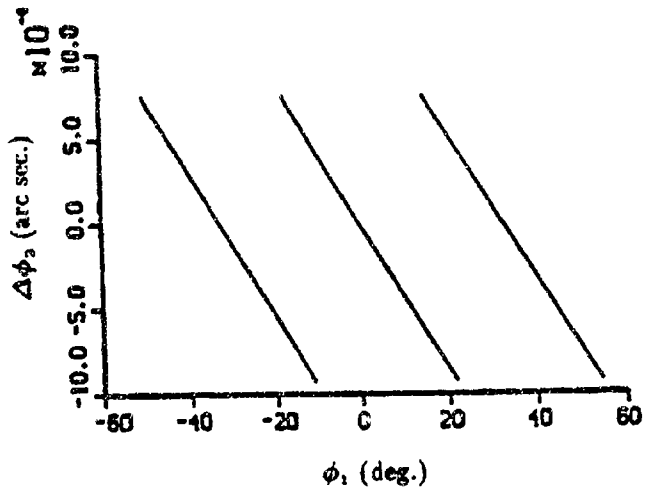

Figure 44: Transmission errors: H=0.01mm (Concave side)

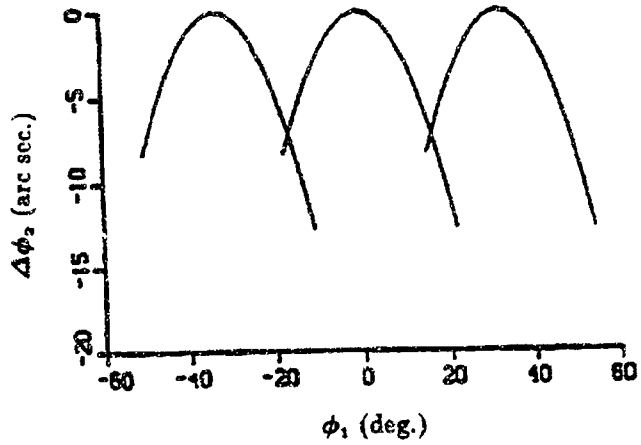

Figure 45: Resulting transmission errors: H=0.01mm (Convex side)

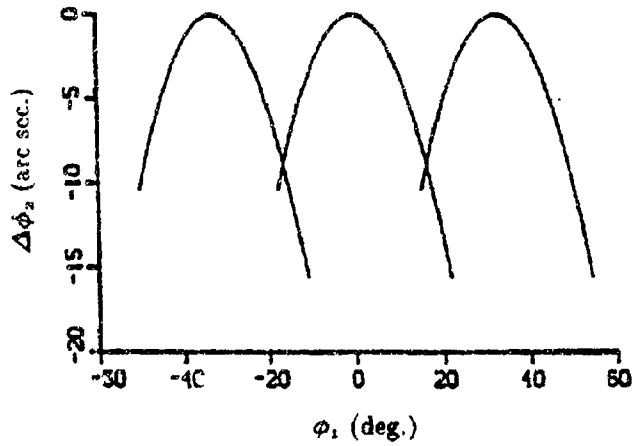

Figure 46: Resulting transmission errors: H=0.01mm (Concave side)

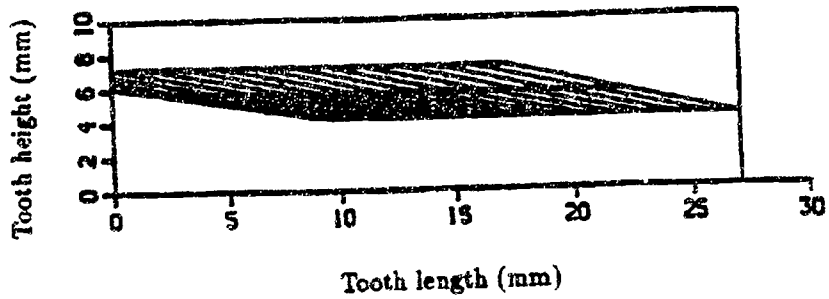

Figure 47: Shift of bearing contact: H=0.01mm (Convex side)

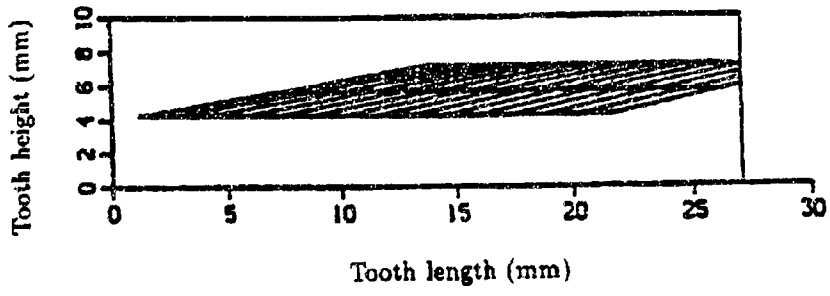

Figure 48: Shift of bearing contact: H=0.01mm (Concave side)

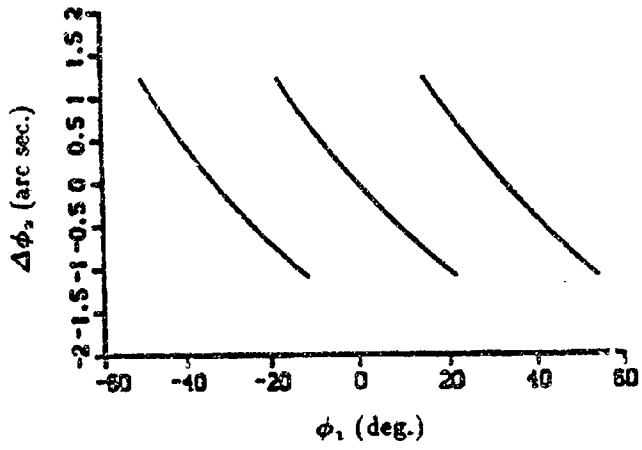

Figure 49: Transmission errors: Q=0.01mm (Convex side)

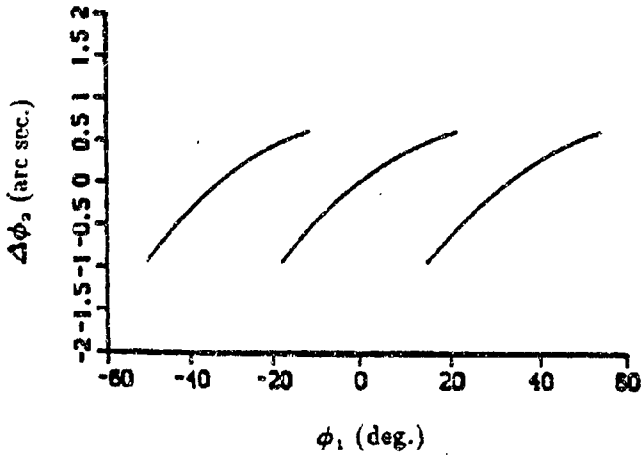

Figure 50: Transmission errors: Q=0.01mm (Concave side)

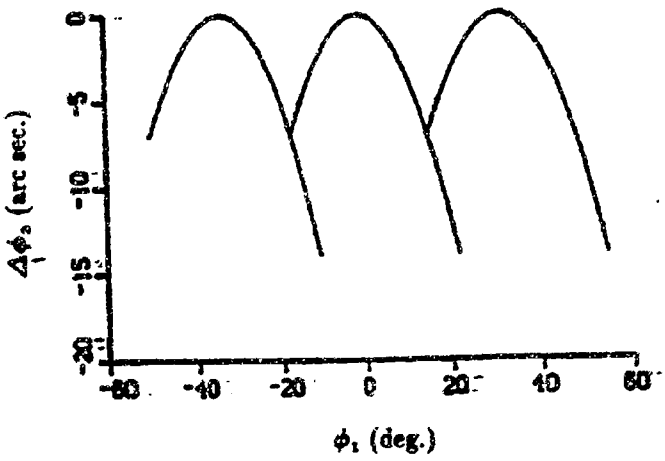

Figure 51: Resulting transmission errors: Q=0.01mm (Convex side)

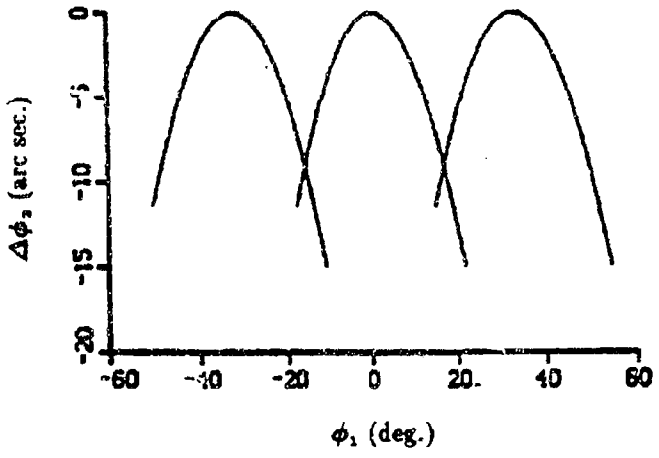

Figure 52: Resulting transmission errors: Q=0.01mm (Concave side)

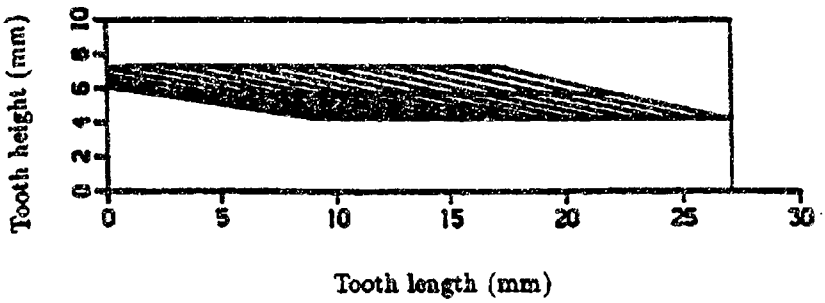

Figure 53: Shift of bearing contact: Q=0.01mm (Convex side)

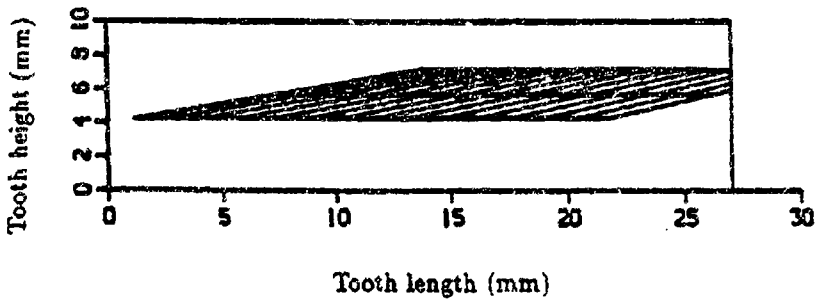

Figure 54: Shift of bearing contact: Q=0.01mm (Concave side)

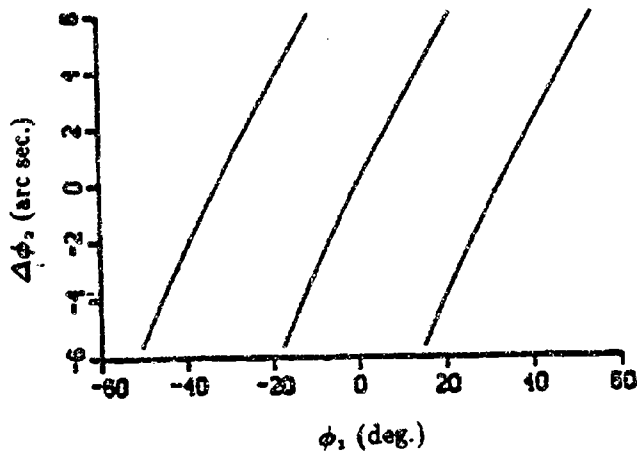

Figure 55: Transmission errors: V=0.01mm (Convex side)

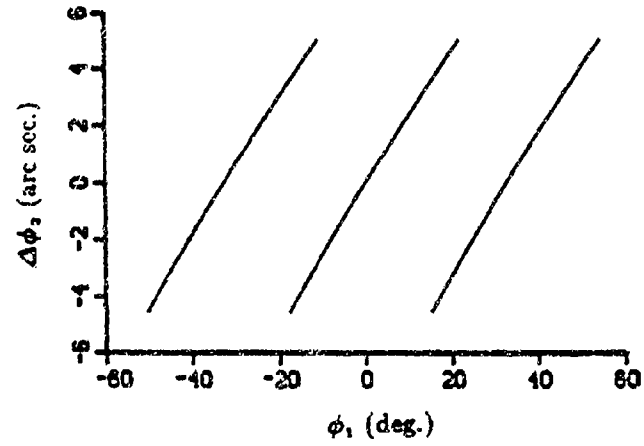

Figure 56: Transmission errors: V=0.01mm (Concave side)

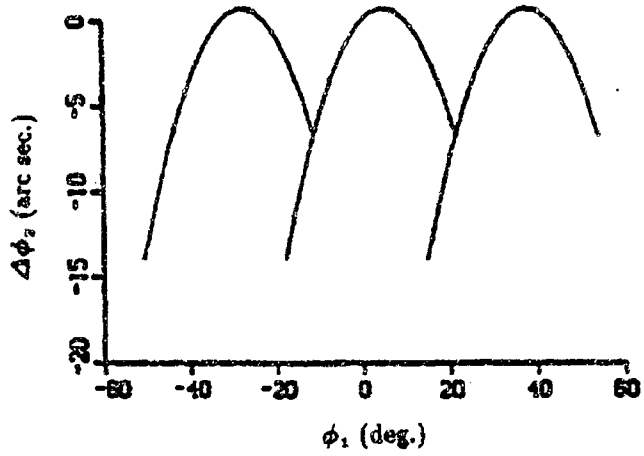

Figure 57: Resulting transmission errors: V=0.01mm (Convex side)

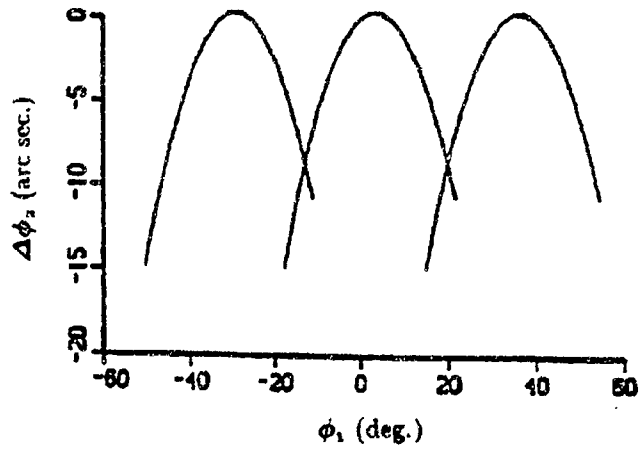

Figure 58: Resulting transmission errors: V=0.01mm (Concave side)

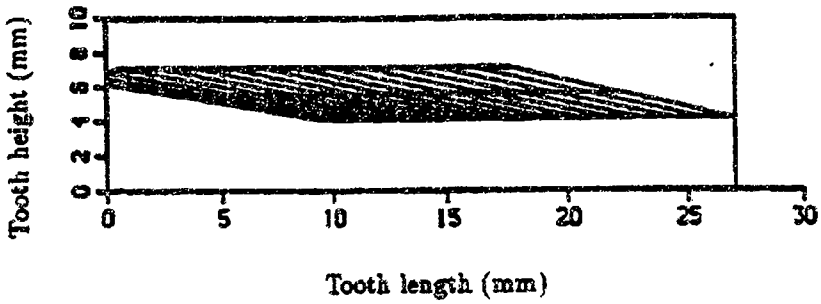

Figure 59: Shift of bearing contact: V=0.01mm (Convex side)

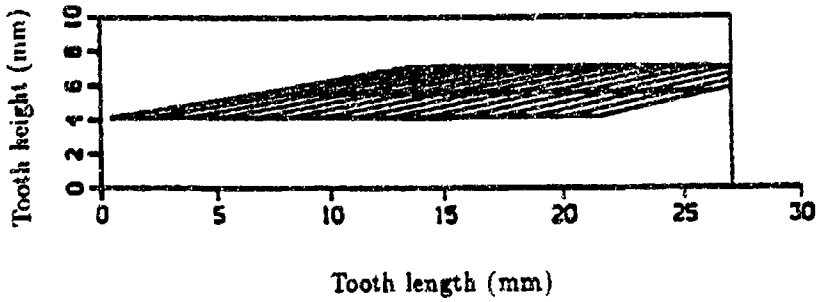

Figure 60: Shift of bearing contact: V=0.01mm (Concave side)

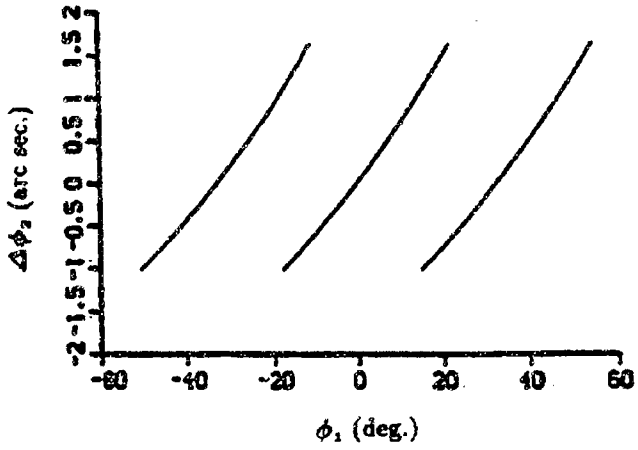

Figure 61: Transmission errors: δ'=1 arc min. (Convex side)

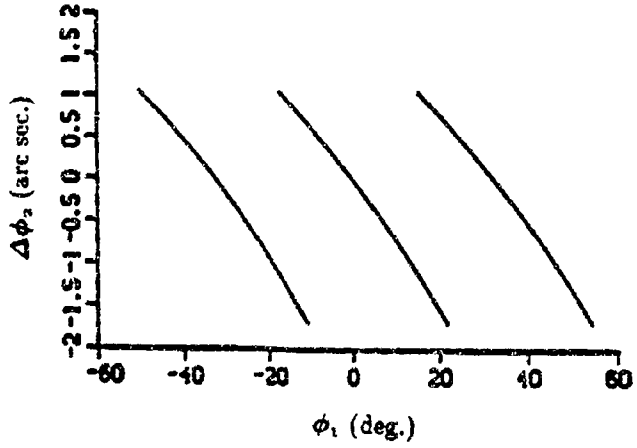

Figure 62: Transmission errors: δ'=1 arc min. (Concave side)

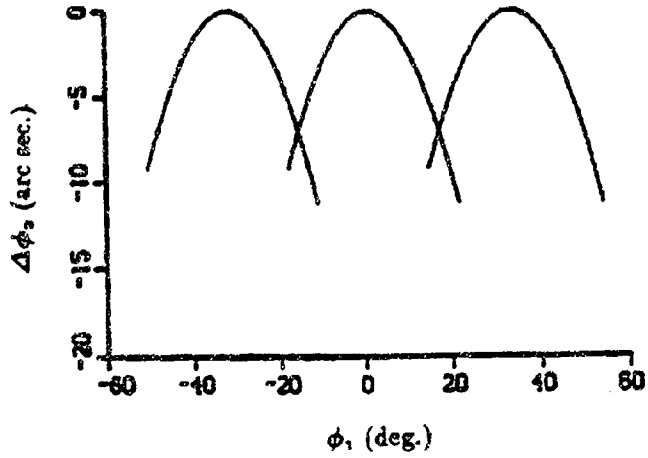

Figure 63: Resulting transmission errors: δ'=1 arc min. (Convex side)

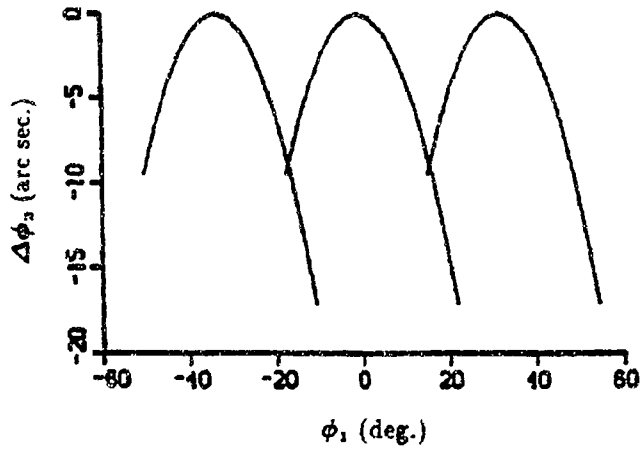

Figure 64: Resulting transmission errors: δ'=1 arc min. (Concave side)

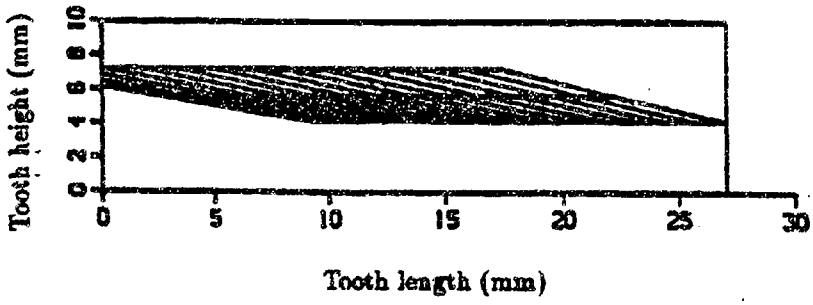

Figure 65: Shift of bearing contact: δ'=1 arc min. (Convex side)

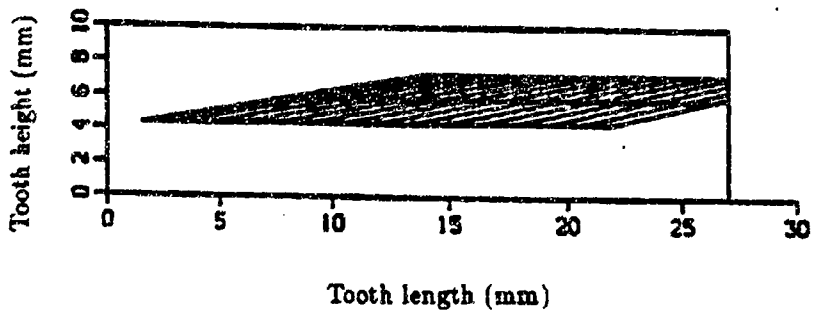

Figure 66: Shift of bearing contact: δ'=1 arc min. (Concave side)

REPORT DOCUMENTATION PAGE

Form Approved
OMB No. 0704-0188

1. AGENCY USE ONLY (Leave blank)	2. REPORT DATE	3. REPORT TYPE AND DATES COVERED
	January 1996	Final Contractor Report

4. TITLE AND SUBTITLE

Computerized Design and Analysis of Face-Milled, Uniform Tooth Height, Low-Noise Spiral Bevel Gear Drives

5. FUNDING NUMBERS

WU-505-62-36
NAG3-1607
1L162211A47A

6. AUTHOR(S)

F.L. Litvin and X. Zhao

7. PERFORMING ORGANIZATION NAME(S) AND ADDRESS(ES)

University of Illinois at Chicago
Chicago, Illinois 60680

8. PERFORMING ORGANIZATION REPORT NUMBER

E-10086

9. SPONSORING/MONITORING AGENCY NAME(S) AND ADDRESS(ES)

Vehicle Propulsion Directorate
U.S. Army Research Laboratory
Cleveland, Ohio 44135-3191
and
NASA Lewis Research Center
Cleveland, Ohio 44135-3191

10. SPONSORING/MONITORING AGENCY REPORT NUMBER

NASA CR-4704
ARL-CR-287

11. SUPPLEMENTARY NOTES

Project Manager, Robert F. Handschuh, Vehicle Propulsion Directorate, U.S. Army Research Laboratory, NASA Lewis Research Center, organization code 2730, (216) 433-3969.

12a. DISTRIBUTION/AVAILABILITY STATEMENT

Unclassified - Unlimited
Subject Category 37

This publication is available from the NASA Center for Aerospace Information, (301) 621-0390.

12b. DISTRIBUTION CODE

13. ABSTRACT *(Maximum 200 words)*

A new method for design and generation of spiral bevel gears of uniform tooth depth with localized bearing contact and low level of transmission errors is considered. The main features of the proposed approach are as follows: (1) The localization of the bearing contact is achieved by the mismatch of the generating surfaces. The bearing contact may be provided in the longitudinal direction, or in the direction across the surface. (2) The low level of transmission errors is achieved due to application of nonlinear relations between the motions of the gear and the gear head-cutter. Such relations may be provided by application of a CNC machine. The generation of the pinion is based on application of linear relations between the motions of the tool and the pinion being generated. The relations described above permit a parabolic function of transmission errors to be obtained that is able to absorb almost linear functions caused by errors of gear alignment. A computer code has been written for the meshing and contact of the spiral bevel gears with the proposed geometry. The effect of misalignment on the proposed geometry has also been determined. Numerical examples for illustration of the proposed theory have been provided.

14. SUBJECT TERMS	15. NUMBER OF PAGES
Gears; Power transmission; Gear geometry	82
	16. PRICE CODE: A05

17. SECURITY CLASSIFICATION OF REPORT	18. SECURITY CLASSIFICATION OF THIS PAGE	19. SECURITY CLASSIFICATION OF ABSTRACT	20. LIMITATION OF ABSTRACT
Unclassified	Unclassified		

NSN 7540-01-280-5500

Standard Form 298 (Rev. 2-89)
Prescribed by ANSI Std. Z39-18
298-102